

# AERODYNAMICS OF HIGH-SPEED TRAINS

---

Joseph A Schetz

*Aerospace and Ocean Engineering Department, Virginia Polytechnic Institute and State University, Blacksburg, Virginia 24061; e-mail: ptiger@vt.edu*

**Key Words** aerodynamics, ground vehicles, Maglev trains

■ **Abstract** This review highlights the differences between the aerodynamics of high-speed trains and other types of transportation vehicles. The emphasis is on modern, high-speed trains, including magnetic levitation (Maglev) trains. Some of the key differences are derived from the fact that trains operate near the ground or a track, have much greater length-to-diameter ratios than other vehicles, pass close to each other and to trackside structures, are more subject to crosswinds, and operate in tunnels with entry and exit events. The coverage includes experimental techniques and results and analytical and numerical methods, concentrating on the most recent information available.

## 1. INTRODUCTION

Interest in the aerodynamics of trains goes back many years. Although the aerodynamics of trains is obviously related to the aerodynamics of other vehicles, there are various important differences. For example, the aerodynamics of airplanes also involves consideration of streamlined bodies, but trains operate near the ground, have much greater length-to-diameter ratios, pass close to adjacent structures and each other, are more subject to crosswinds, and travel at lower speeds. Trains on some routes operate in numerous tunnels, with consequent tunnel entry and exit events. Automobiles and trucks also operate near the ground, pass each other, and are subject to crosswinds, but trains have much greater length-to-diameter ratios and their speeds are higher. These and other differences are discussed in this review, with the emphasis on modern, high-speed trains.

In his overview of early work on train resistance, Muhlenberg (1978) cites formulas published by Schmidt in the United States in 1910, Strahl in Germany in 1913, and Mukhachev in Russia in 1927 and mentions that similar formulas were developed in England and France during the same time period. For many years, the Davis formula, published in 1926, and later modifications to it were widely used (Muhlenberg 1978). These formulas for trains in the open are all of the general form

$$R = A + (B_1 + B_2)V + CV^2, \quad (1a)$$

where  $R$  is the total resistance to motion and  $V$  is the train speed in still air. When ambient winds are appreciable, the formula is modified as

$$R = A + B_1 V_G + B_2 V_A + C V_A^2, \quad (1b)$$

with  $V_G$  as the train speed relative to the ground and  $V_A$  as the train speed relative to the air.

The coefficient  $A$  is the rolling mechanical resistance; Gawthorpe (1978) cites  $A/m$  as 0.008–0.02 N/kg of train mass.  $B_1$  is other mechanical resistance, such as transmission losses and brake drag. Gawthorpe (1978) cites  $B_1/m$  as  $1.5\text{--}2.0 \times 10^{-4}$  N/kg of train mass per m per s of train speed.  $B_2$  is air momentum drag associated with the energy required to accelerate the mass of air ingested for combustion, engine cooling, and air conditioning. Again, Gawthorpe (1978) gives  $B_2/L$ , where  $L$  is the train length, as 0.2–0.25 kg/s per m of train length per m per s of train speed. Finally, we come to external aerodynamic resistance, which is mainly expressed in terms of the coefficient  $C$ :

$$C V_A^2 = \frac{1}{2} \rho V_A^2 S C_D. \quad (2)$$

Here,  $\rho$  is the density,  $S$  is the frontal area of the train, and  $C_D$  is the drag coefficient. Values of  $C_D$  for  $S$  on the order of  $10\text{ m}^2$  and  $L$  on the order of 300 m can range from  $\sim 1.0$ , or somewhat less, for highly streamlined trains to  $\leq 10\text{--}15$  for freight trains. Because much of the aerodynamic drag results from skin friction, which depends upon Reynolds number ( $Re$ ), the total aerodynamic drag is proportional to a power somewhat less than 2. Thus, some of the skin friction drag should be included in  $B_2$ , and extrapolations of data to high speeds assuming a  $V^2$  dependence will be overly pessimistic.

For streamlined trains at speeds of  $\sim 250\text{--}300$  km/h, 75–80% of the total resistance is caused by external aerodynamic drag (Gawthorpe 1978). About 30% of this external aerodynamic drag is caused by skin friction, about 8–13% by nose and tail pressure drag, 38–47% by bogie and associated interference drag, and 8–20% by pantograph and roof equipment drag (Peters 1983). Clearly, as one begins to consider trains that operate at much higher speeds, such as those that use magnetic levitation (Maglev) or other advanced concepts, external aerodynamics must be a major consideration.

This introduction has only considered aerodynamic drag and the simplest case of isolated trains operating in open air, on level grades, with no wind. That case is discussed in more depth below, as are the important effects of (a) winds, especially crosswinds; (b) operations in tunnels; (c) trains passing each other or stationary structures; and (d) aerodynamic noise, as well as combinations of some of these effects. The last section discusses some of the special aerodynamic issues raised by Maglev trains. Some consideration also is given to lift, side force, and moments as well as flowfield details where information is available. In each section, experimental information from both full-scale and laboratory-scale sources is covered first, followed by a discussion of simplified analyses and then complex computational fluid dynamic (CFD) models.

## 2. ISOLATED TRAINS IN THE OPEN WITHOUT CROSSWINDS

### 2.1 Experimental Data

The resistance formulas cited above are all based upon a mixture of full-scale track data and sub-scale wind tunnel, water tunnel, towing tank, or test track data. Full-scale track data should be preferred, because scaling and other important issues addressed below are avoided. A dynamometer car can be incorporated into a train consist, which allows the resistance of various parts of the train to be measured. The mechanical resistances are then subtracted from the total resistance to yield the aerodynamic component (Gawthorpe 1978). The coasting technique is often used to determine the total resistance (Bernard & Guiheu 1976) in a manner similar to that for automobiles. In addition to high cost, there are many problems associated with full-scale testing. The most troublesome problem is that of ambient wind conditions, especially crosswinds, because these have a very large effect on aerodynamic resistance.

In light of the problems with full-scale tests, most experimental studies on the aerodynamics of high-speed trains are conducted at sub-scale in laboratory facilities. Under these conditions, the flow can be carefully controlled, but a number of serious issues arise. First, as is the case with aerodynamic tests at sub-scale for any vehicle, proper attention must be given to the appropriate scaling parameters. Ideally, both the  $Re$  and Mach number ( $M$ ) of the model should match that of the full-scale vehicle. If wave-propagation phenomena are not deemed important or are not considered and  $M < 0.2$  under full-scale conditions, then one need only have  $M < 0.2$  in the model scale. If the air speeds relative to the train are approximately the same in both the model and full-scale train, then the  $Re$  in the laboratory will obviously be much less than that for a full-scale vehicle in the ratio of the model- to full-scale length dimensions. This problem is a familiar one for model testing of all vehicles, and it is certainly no less important for trains, which can be very long. Trains have particular problems with testing on models, because they feature a number of important drag-producing smaller-scale items like bogies, pantographs, and gaps between cars. Current thinking is that tests should not be conducted at much less than one-tenth scale (Peters 1983). Baker & Brockie (1991) report that extrapolation of model-scale results to full-scale vehicles can lead to 30% errors in  $C_D$ . Willemssen (1997) found better agreement ( $\sim 10\%$  error) when extrapolated data from the German-Dutch high- $Re$  wind tunnel was compared with full-scale results.

A challenging problem for wind and water tunnel tests of any ground vehicle is proper simulation of the significant effects produced by the nearby ground plane or track. In the simplest real case, the ground and air are at rest and the vehicle moves. In a wind or water tunnel, the ground and the vehicle model are at rest and the air (or water) moves past. The resulting flowfields for the two cases are different. The flow visualization in the movies from ONERA (Office

National d'Études et de Recherches Aérospatiales; Werle 1969) offers a convincing demonstration of that fact. Some efforts have been made to simulate these effects by removing the tunnel wall boundary layer by suction or by using two models in a "mirror-image" arrangement, but the most satisfactory method by far is to use a moving tunnel wall in the form of a belt. The belt speed must match the tunnel speed, which is more challenging for high-speed train testing than in automobile model testing. Baker & Brockie (1991) report that different types of wind tunnel ground simulation can produce  $\leq 10\%$  differences in drag. The effects on lift can also be large, and lift can be important for Maglev vehicles, for example.

One can now ask what kind of wind tunnel can be used to obtain useful results for the aerodynamics of high-speed trains. One reference point is the SNCF (Société Nationale des Chemins de Fer Français)  $2.2 \times 1.75 \times 15$  m wind tunnel with a moving ground belt at the Institut Aerotechnique of Saint-Cyr (Bernard 1973). Good agreement between model test results from that facility and the results from the full-scale coasting tests of the French high-speed train à grande vitesse (TGV) train has been reported (Guiheu 1982).

Some of the problems described above can be alleviated by testing with a moving vehicle on a track. A towing tank of the type used for ship-model testing is useful here, and good results have been obtained at the Institute for Shipbuilding in Hamburg with an inverted model towed near the tank floor. Obviously, cavitation must be avoided. An innovative test facility has been developed by British Rail Research (Pope 1991) that uses 1/25th-scale models moving along 136-m tracks, as illustrated in Figure 1. Rubber launchers are used to propel the models, and when they reach the end of the test section, a hook engages a cable connected to a piston in a cylinder for braking.

Some special test facilities have also been built for studying the effects of crosswinds, tunnel entry and exit, and other phenomena, but discussion of those facilities is deferred until later in this review.

Looking now at some experimental results for various drag components, we consider first the pressure drag on the nose and tail sections. Thorough studies (e.g. Mackrodt et al 1980, Mackrodt 1980) have shown that there is no significant difference in drag produced by a large variety of slender shapes, if sharp edges are avoided. A typical pressure distribution obtained from a wind tunnel test is compared with predictions from an inviscid panel method in Figure 2. The effects of the nose (and tail) shape on the overall drag of a train are quite small, because the contribution to the total drag by pressure drag is small and the drag caused by the nose and tail are governed more by the underbelly flow than by the flow over the exposed surfaces. In addition, high-speed trains are almost always designed to be bidirectional, with identical leading and trailing cars, so the nose and tail shape are assumed to be the same. The shape of the tail is also thought to be less important, because it operates deep in the thick turbulent boundary layer that develops along the length of the train.

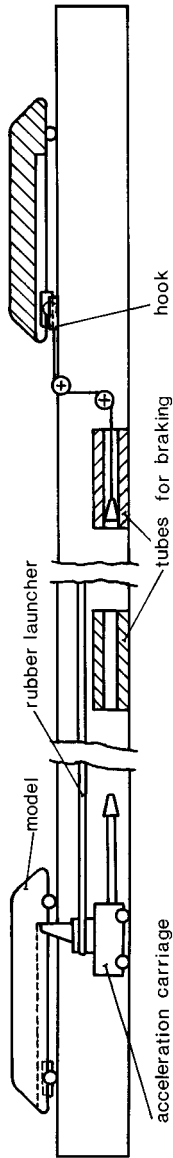


**Figure 1** Moving model test facility built by British Rail Research. (From Sockel 1996. Reprinted by permission.)

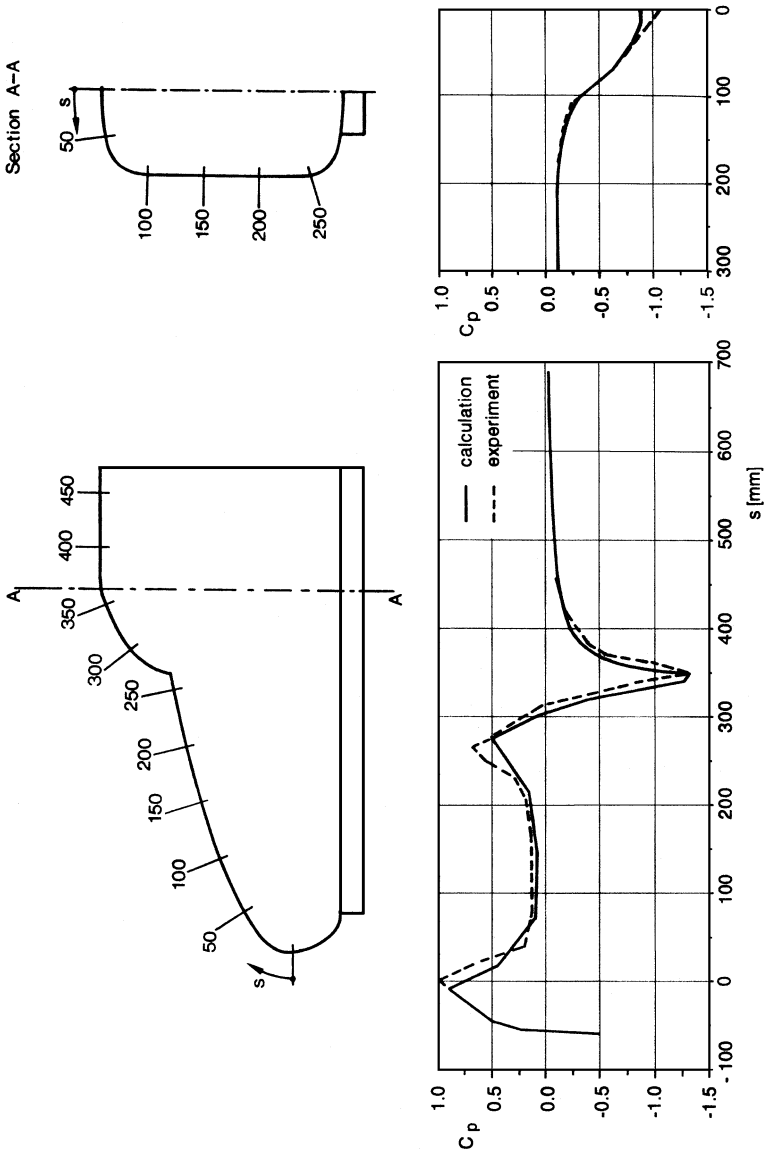


**Figure 2** Measured and calculated pressure distributions on a train nose model. (From Mackrodt et al 1980.)

Next, we consider the turbulent boundary over the train and its effects on drag. Flow data report a range for  $C_f$  ( $C_f \equiv \tau_w / \frac{1}{2} \rho V^2$ , where  $\tau_w$  is the wall shear) from a high of 0.006 to as low as  $\sim 0.001$  (Sockel 1996). The flow over a train is very three-dimensional, so the values vary markedly along and around the vehicle. Brockie & Baker (1990) recommend values of 0.002–0.004. Sockel (1996) gives results for measurements of boundary-layer thickness ( $\delta$ ) along various train bodies, shown in Figure 3. These results show that the boundary layer displacement thickness ( $\delta^*$ ) ranges from  $\delta/8$  to  $\delta/12$ . Boundary layer profiles were measured along a train model on a moving track by Baker et al (1999), and they report that the shape factor ( $H = \delta^*/\theta$ , where  $\theta$  is the momentum thickness) is relatively constant at a value just above 1.0 for the length of the train. Paradot et al (1999) provide boundary layer profiles along the roof as well as the velocity distribution in a cross-plane behind a TGV model over a moving belt in a wind tunnel, as shown in Figure 4.

The drag breakdown cited in section 1 attributed the bulk of the aerodynamic drag to such items as the bogies, pantographs, etc, so careful attention must be directed to those areas. All modern high-speed trains incorporate such obvious aerodynamic refinements as smooth skin, flush windows and doors, carefully designed intercar spaces, and underfloor fairings. The aerodynamic design of bogies is an area that has continued to receive attention (Schulte-Werning et al 1999b). It is reported that the drag caused by the bogies can be reduced by  $\leq 20\%$  by aggressive application of deflectors under the nose, skirts and underbelly fairings, fairings over the bogies, and nonprotruding bogies.

For high-speed trains using electric propulsion, the aerodynamics of the pantograph are an important matter. The issues concern not only drag but also lift,

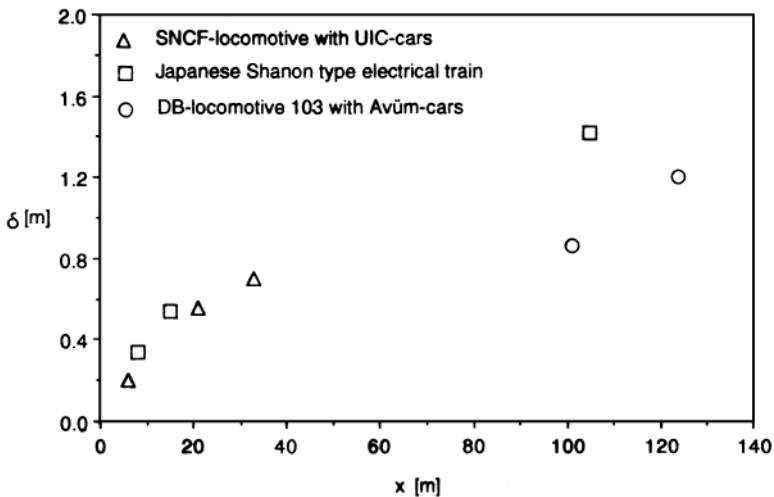
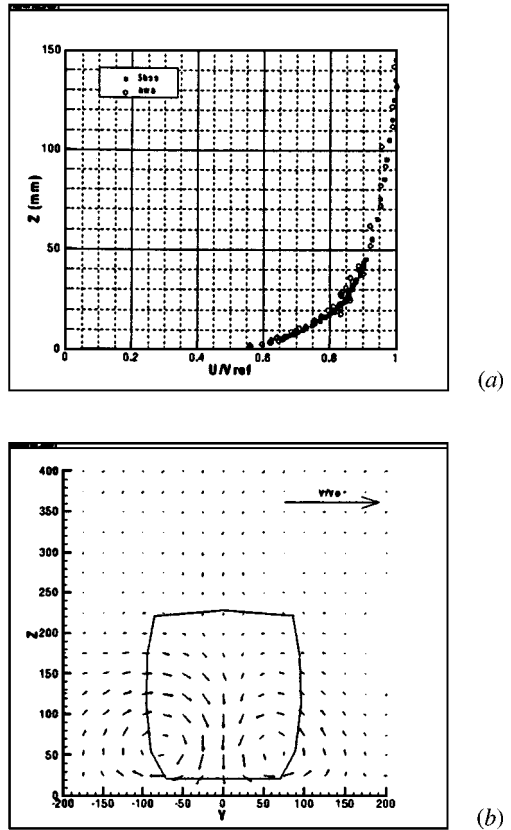


**Figure 3** Measured boundary layer thickness distributions on the walls of trains at the height of the windows. (From Sockel 1996. Reprinted by permission.)

**Figure 4** Measured velocity distributions near a TGV model in a wind tunnel. (a) Boundary layer profiles on the roof at  $x = 4407$  mm. (b) Cross-flow velocities in the wake 300 mm behind the tail. (From Paradot et al 1999, with permission of Railroad Technical Research Institute.)



because lift affects the wire contact force. The best practice is to use pantographs that have a neutral lift. Representative works may be found in Althammer et al (1999). Fairings can reduce the drag by  $\sim 50\%$ , and telescoping pantographs can reduce the drag by  $\sim 90\%$  (Peters 1983).

High-speed trains that use combustion engines for propulsion have special aerodynamic problems involving the design of the intake, exhaust, and cooling systems. Much of the technology in this area stems from work in nonrailway fields such as automobiles. Intake design is constrained by the need to operate while the train is moving in either direction. The need to prevent exhaust reingestion usually leads to intakes being located on the train underbelly or sides, with the exhaust on the roof. These locations also help prevent rain, dust, and debris ingestion and reduce exhaust noise and pollution problems. At speeds greater than  $\sim 150$  km/h, it has been found that the intake should not be located closer than 1.5 body widths from the nose or in roof corner regions (Gawthorpe 1978).

## 2.2 Analysis

There are essentially two levels of analyses available. The first consists of simple data correlations of the type described in section 1. The second involves computer-based treatments that are either of the inviscid, panel method type or of the complex CFD class that uses the turbulent, Re-averaged, Navier-Stokes (RANS) equations.

For the analyses based on data correlations, the drag coefficient,  $C_D$ , is broken down as (Sockel 1996)

$$C_D = C_{DL} + C_B + \lambda_T(l_T - l_L)/A^{1/2}, \quad (3)$$

where  $C_{DL}$  is the drag coefficient of the leading car or locomotive;  $C_B$  is the base drag at the vehicle tail;  $\lambda_T$  is the friction along the train, which includes the bogies, wheels, interference, underbelly effects, etc; and  $l_T$  and  $l_L$  are the length of the total train and the lead car, respectively. Sockel (1996) has compiled typical values of these parameters, which are given in Table 1.

The simplest type of computer-based analysis is of the inviscid, panel method class, and we have already seen a representative comparison of prediction vs measurement using this method in Figure 2. The comparison looks good, but the agreement deteriorates rapidly in the presence of a crosswind. Also, such inviscid methods obviously cannot predict viscous drag, and we have seen that drag is important for high-speed trains that have a streamlined shape and high  $l_T/A^{1/2}$ . Gaylard provides a review of CFD work for trains prior to 1993 (Gaylard 1993),

**TABLE 1** Typical drag and friction coefficients for trains<sup>a</sup>

Train type <sup>b</sup>	$C_D(0)$	$A_T$ (m <sup>2</sup> )	$l_T$	$l_L^c$	$C_B^c$	$C_{DL}^c$	$\lambda_T$	Reference
APT-P	2.05	8.05	300	13.0	0.11*	0.2*	0.0172	Gawthorpe 1978
HST	2.11	9.12	300	17.4	0.11*	0.2*	0.0192	Gawthorpe 1978
Conventional passenger train MKII	2.75	8.8	300	20*	0.11*	0.3*	0.0248	Gawthorpe 1978
Container 80% loaded	6.5	8.8	300	20*	0.11*	0.5*	0.0624	Gawthorpe 1978
Shinkansen 200	1.52	13.3	300	24.5	0.11	0.2	0.0160	Maeda et al 1989
ICE	0.69	10.2	115	20.9	0.12	0.2	0.0125	Peters 1990b

<sup>a</sup>From Sockel 1996.

<sup>b</sup>APT-P, advanced passenger train; HST, high-speed train; ICE, InterCity Express.

<sup>c</sup>Asterisk indicates estimated values.

and he cites reasonable agreement between predictions based on panel methods and pressure data for cases without crosswinds. The application of viscous CFD codes to railway aerodynamic problems began in earnest in the early 1980s (Gaylard 1993).

The RAPIDE project (Schulte-Werning et al 1999a) involves CFD and model- and full-scale testing for validation. Some interesting recent results for the 205-m-long InterCity Express(ICE)-2 train at 280 km/h are available in Matschke et al (1999a). The CFD with commercial RANS- $k\epsilon$  codes using wall functions was conducted in three parts by three groups of investigators. Some results, including a comparison with wind tunnel data, are given in Figure 5.

### 3. EFFECTS OF CROSSWINDS

Crosswinds have many important effects on the aerodynamics of trains. One might, perhaps, expect that the increase in operating speed of modern high-speed trains would reduce the effective yaw angle that corresponds to a given crosswind component, so that the effects would be reduced. However, high-speed operation of modern trains has been accompanied by a significant reduction in train weight as a result of better structural design and improved materials, so the net effect has been an increase in the importance of crosswind effects.

The simplest effect of a crosswind is on aerodynamic drag. The crosswind velocity combined with the velocity of the train produces a yaw angle,  $\beta$ , and a simple correction to the drag coefficient for a modern train shape has been developed (Peters 1990a) for  $\beta < 30^\circ$ :

$$C_D(\beta) = C_D(0)(1 + 0.02\beta). \quad (4)$$

Gawthorpe (1983) estimates that the average daily wind adds  $\sim 10\%$  to the aerodynamic drag on a calm day and  $\sim 50\%$  on a windy day for a train operating at 160 km/h in a Beaufort Scale Force 8 gale crosswind. Peters (1983) concludes that for a train operating at 250–300 km/h in a wind of 15 m/s, the worst condition arises for a wind angle of  $30^\circ$ , which results in a 60% increase in drag.

Data on the effects of a crosswind not only on drag but also on lift, side force, and moments are very important for assessing vehicle stability. Interest in this subject has increased recently with the introduction of unpowered, lightweight, high-speed vehicles placed in the lead position of a train (Heine & Matschke 2000). Strong gusts cause a deloading of the wheels on the windward side. A train that encounters a gust just as it leaves a tunnel is in a particularly difficult situation.

#### 3.1 Experimental Data

Some data can be obtained from full-scale tests, even though this is an expensive and complex undertaking. Results of such tests have been reported by Heine &

Matschke (2000). Rolling-moment data are given in Figure 6 for various configurations of the train, the embankment, and a noise barrier.

Laboratory tests allow specification of conditions that are more repeatable and make measurements easier, but critical issues of scaling and simulation arise. For example, blockage effects of a long model at yaw in a wind tunnel are clearly greater. In addition, if the moving-belt method of simulating ground plane effects is used, should the moving belt be yawed as well as the model? That change would lead to mechanical complexity and the issue of the disturbance produced by the now exposed edge of the moving belt. Indeed, matters are more complex with regard to simulation of the ground plane (Gawthorpe 1994), because many of the most troublesome locations for crosswind effects are on exposed embankments or viaducts. The vehicle may be operating in a 90° crosswind at an effective yaw angle of 40° when considering forward motion, which would require that the vehicle be set at 40° yaw in the wind tunnel. However, the fixed embankment is subjected to a 90° crosswind, and it can only be modeled in the wind tunnel as yawed at 40°, the same as the train. There is also the matter of properly simulating the atmospheric boundary layer on a laboratory scale. This problem has received considerable attention in studies of wind loads on buildings, and Cooper (1984) gives relevant information for tests of ground vehicles. These considerations have led to wind tunnel test approaches at two extremes. The first approach uses a relatively large-scale model at yaw in a wind tunnel placed on a fixed, elevated ground board. This gives a reasonable  $Re$  level, but the moving ground plane and the atmospheric boundary layer are not represented. The second approach uses a small-scale model

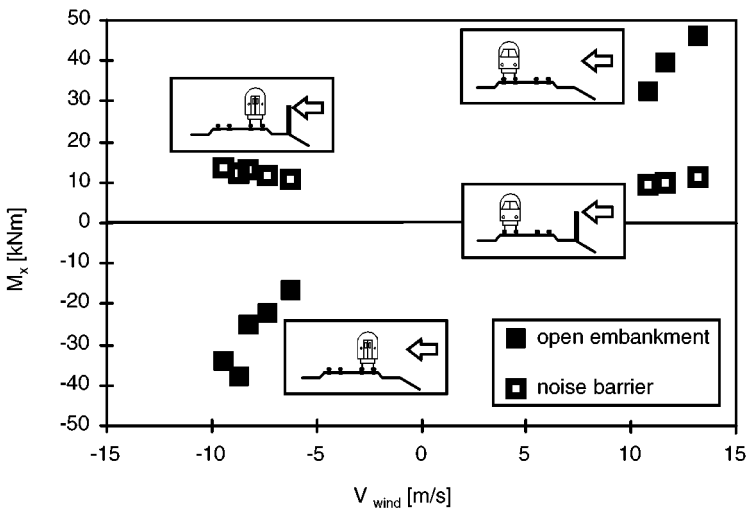


**Figure 6** Rolling moment measurements on the InterRegion train vs wind velocity for various train and trackside arrangements. (From Heine & Matschke 2000, with permission of TRANSAERO Consortium.)

set on a fixed floor exposed to an elaborately simulated atmospheric boundary layer. Many of the concerns about crosswinds center around unsteady gusts. Bearman & Mullarkey (1994) describe a wind tunnel test that used a flapping airfoil to produce gusts, and Dominy & Docton (1994) used an unsteady cross jet in an open-throat wind tunnel to produce gusts; both groups were working on road vehicle testing.

All of these considerations have led to various moving-model laboratory test arrangements. We have already seen one version of this in Figure 1, and train model testing in a towing tank has also been mentioned. The idea is to launch a model along a track on a ground surface in a wind tunnel, over which a simulated atmospheric boundary layer is flowing. The ground plane and the crosswind are properly simulated relative to the moving train model. There are new test problems that focus on the need to have a smooth, accurately aligned track to assure smooth motion of the model, or the model load balance will have difficulty distinguishing the aerodynamic loads on the model from dynamic inertia forces fed up from the track (Gawthorpe 1994).

Baker & Humphreys (1996) attempted to reach some conclusions about the effects of the various types of wind tunnel simulations on aerodynamic force data, but they focused on sharp-edged vehicle shapes. They concluded first that results for mean side-force coefficients on ground vehicles in a crosswind are insensitive to the nature of the wind tunnel simulation. Vehicles with rounded edges will likely show a greater dependence on  $Re$ . On the other hand, Baker & Humphreys found that lift coefficients are very dependent on the test arrangement and conditions. High  $Re$  and a moving model are recommended.

The aerodynamic rolling moment, which is of great interest for train stability, has been found to arise mainly from the side force, with a small contribution from the lift. The rolling-moment variation with yaw angle for a high-speed train design is presented in Figure 7. The pressure distribution on the lead car produces a larger effect than for subsequent cars. There is a linearly increasing regime for yaw angles up to about  $45^\circ$  and a constant-value regime for higher angles.

Wind tunnel tests can be used to set limits on train operation in crosswinds (Krönke & Sockel 1994). Peters (1990b) and Baker & Humphreys (1991) conclude that wind tunnel data from tests without atmospheric turbulence should be applied with care.

Studies on the gross effects of a crosswind on trains, including operation on embankments and bridges, and various means of minimizing problems with the use of barriers continue (Baker 2000, Suzuki et al 1999).

The effects of crosswinds on train aerodynamics are not limited to the main vehicle. For electric-powered trains, crosswinds can cause the conductor wire above the track and/or the train pantograph (Gawthorpe 1994) to malfunction. The failure is usually the result of increased lift on the pantograph in a crosswind; the pantograph then tries to push itself up through the wire system.

Wind tunnel experiments have shown that there are two yaw angle regimes, which are distinguished by differing vortex patterns on the leeward side of the train. At a yaw angle up to  $\sim 45^\circ$ , a system of inclined vortices are formed like

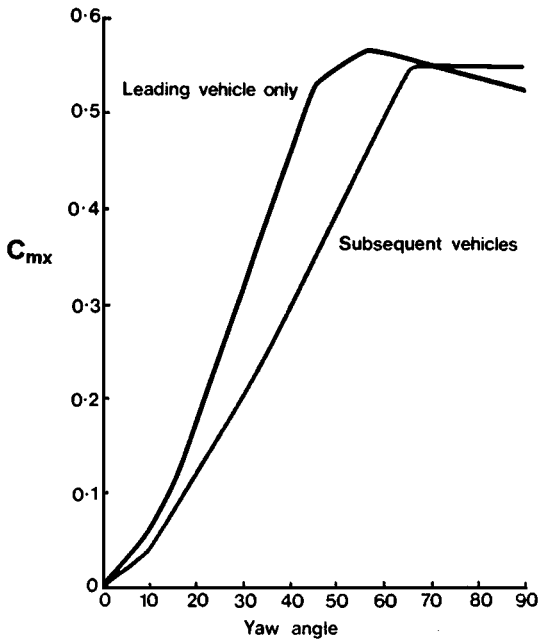


**Figure 7** Rolling moment characteristics for a train in a crosswind. (From Gawthorpe 1994, with permission from Elsevier Science.)

those found on slender bodies in general. These vortices are shed from the train roof and the ground surface boundary layers. The vortices are then detached from the train, and new ones are formed. At a yaw angle greater than  $\sim 60^\circ$ , the flow on the lee side resembles that behind a circular cylinder in a crossflow. Between  $\sim 45^\circ$  and  $60^\circ$ , the flow fluctuates between these two patterns (Chiu & Squire 1992). Figure 8 presents surface flow patterns that were deduced from oil-flow studies on a train model attached to a ground board in a wind tunnel at  $60^\circ$  of yaw by Chiu & Squire (1992).

### 3.2 Analysis

A typical, simple data correlation result was given above in Equation 4.

Copley (1987) applied panel methods for a train model operating at yaw and provided some comparisons with wind tunnel observations. Near the nose of a train of modern design at  $25^\circ$  yaw, a conventional three-dimensional panel method provides good predictions, because there is little separation and the wake further downstream has little effect. For larger yaw angles and/or stations further along the train, the separated flow on the lee side must be modeled. This is difficult using panel methods unless the separation locations are obtained by means of experiment or separate boundary layer calculations and incorporated into the calculation. The region farther along the train can often be successfully modeled as two-dimensional for high yaw angles. See Copley (1987) and

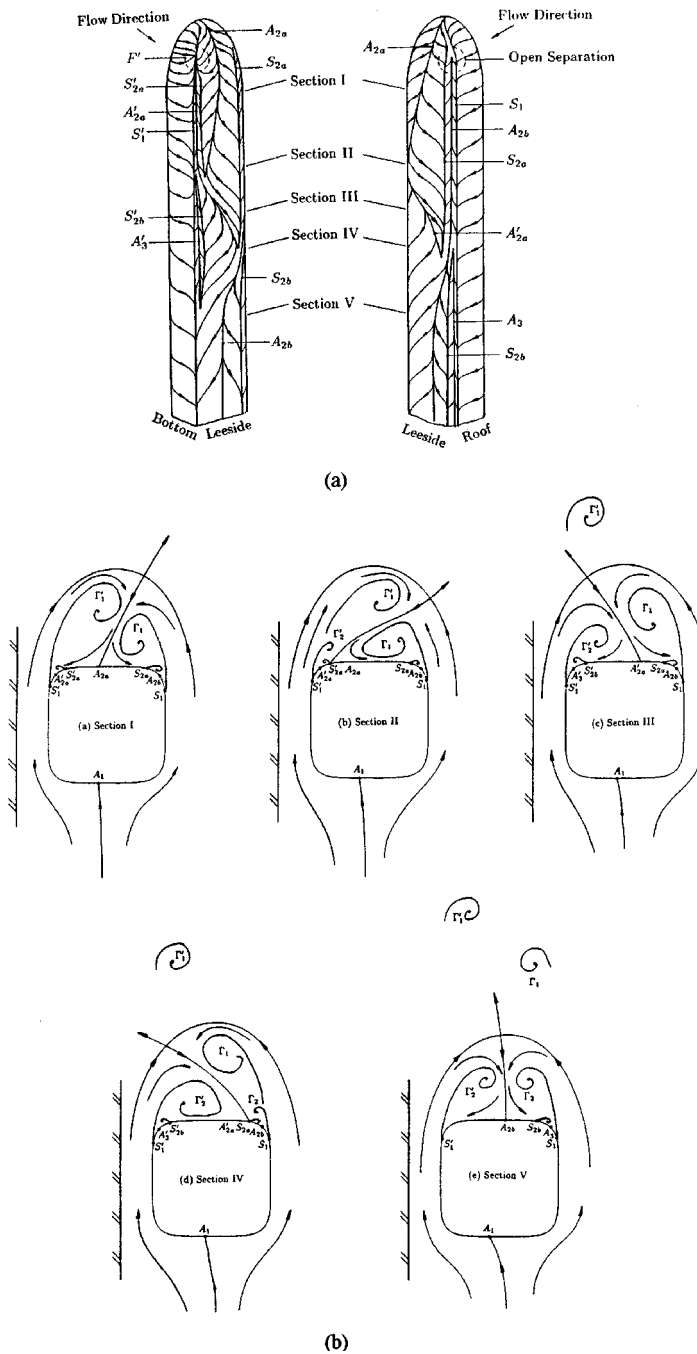


**Figure 8** Observations of vortex wakes from a train model in a crossflow. (a) Surface flow patterns, (b) axial development of the wake. (From Chiu & Squire 1992, with permission from Elsevier Science.)

Chiu (1995) for further details on panel method analyses and comparisons of predictions and data for trains.

Modern CFD methods based on RANS and using the  $k\epsilon$  class of turbulence models have been applied to train aerodynamics problems, including crosswinds, since the early 1990s. The earliest works used the two-dimensional approximation that is usually considered to be more or less valid for high-yaw angles like  $90^\circ$  (Gaylard 1993).

The TRANSAERO program (Matschke et al 1999b) uses RANS-based CFD with a renormalization group theory(RNG)- $k\epsilon$  turbulence model, wind tunnel experiments, and full-scale tests to study train aerodynamics, including the effects of crosswinds. The CFD models use up to 8 million cells. Figure 9 compares side-force and rolling-moment results from all three study methods, including two sets of wind tunnel results that correspond to a static and moving model.

#### 4. TRAINS IN TUNNELS

Rail lines for very high speed trains involve more and more tunnels for various reasons, which include (a) environmental considerations in densely populated areas, (b) the increasing scarcity of free flat space, and (c) the desire for straighter tracks for high-speed operation. The aerodynamic consequences of high-speed train operation in tunnels center on two interdependent phenomena, namely, the generation of pressure waves and an increase in drag. In long tunnels the drag increase is the most important effect, whereas in short tunnels the pressure pulses generated at the tunnel entrance and exit cause the most problems.

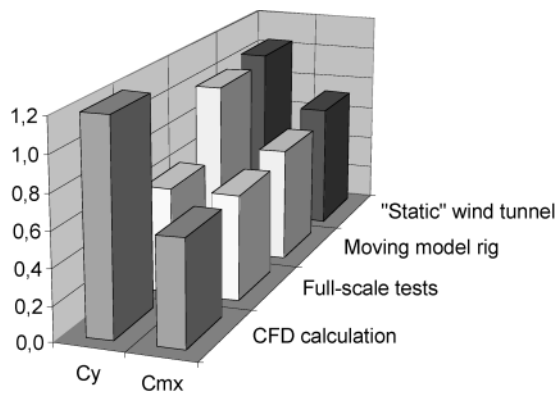


**Figure 9** Comparison of measurements at full-scale and at subscale from a moving and a static model and predictions with a Reynolds-averaged Navier-Stokes computational fluid dynamic (CFD) method for side force and rolling moment for a train in a crosswind. (From Matschke et al 1999b, with permission of Railroad Technical Research Institute).

## 4.1 Aerodynamic Drag in Tunnels

The aerodynamic drag of a train in a tunnel can exceed the drag for the same train in open air by a substantial margin. The effect depends primarily on the blockage ratio of the train in the tunnel ( $R$ ), the length of the tunnel and the train, the shape of the train nose and tail, the presence of air shafts and cross-connections in the tunnel, the roughness of the tunnel wall, the roughness of the train, and the presence of other trains in the tunnel. Experimental studies of train aerodynamics in tunnels can be conducted at full scale (Matsuo et al 1997, Vardy & Reinke 1999) or on models in the laboratory, using the facility shown in Figure 2 (Pope 1991) or the newer, moving-model facility that can launch models up to 500 km/h (de Wolf & Demmenie 1997).

Like any other vehicle, the drag on a train is a combination of pressure drag and skin friction drag, but in a tunnel the magnitudes of the two types of drag are altered compared with operation in the open. Significant pressure waves are generated at the tunnel entrance and exit, and longitudinal pressure gradients develop along the train in the confines of a tunnel. Clearly, the flowfield around the train is altered. In particular, any separation zones just downstream of the nose or on the tail will be strongly affected, which affects nose and tail drag.

The total aerodynamic drag of a train in a tunnel is usually expressed (Vardy 1996a,b) in terms of a nose loss coefficient,  $k_N$ , which implies a stagnation pressure loss as

$$(\Delta p_s)_{\text{Nose}} = k_N (1/2 \rho V_{\text{Nose annulus}}^2), \quad (5)$$

and a tail loss coefficient,  $k_T$ , which implies a stagnation pressure loss as

$$(\Delta p_s)_{\text{Tail}} = k_T (1/2 \rho V_{\text{Tail annulus}}^2). \quad (6)$$

Note that the velocities in the annulus between the train and the tunnel wall will not, in general, be the same at the nose and tail for a long train. Vardy (1996a,b) gives estimates for these coefficients as  $k_N \sim 0.1$  or less for a streamlined nose and  $k_T \leq R^2$ . Gaillard (1979) suggests that the skin friction coefficient in a tunnel is increased compared to that in the open air by a factor  $(1 + 2.21R)$ , but Vardy (1996a,b) points out the difficulties of determining this factor. Vardy (1996a,b) estimates that the ratio of drag caused by friction to that caused by pressure drag from the nose and tail is  $\sim 5.5$  for a typical case.

Gawthorpe et al (1979) used a similar formulation to produce estimates of the important influences of tunnel length, blockage ratio, and train shape on drag. Sockel (1996) presents results restricted to streamlined shapes in long tunnels but includes the important effects of the acceleration of the train and the surrounding air. The ratio  $T_f = C_{DT}/C_D(0)$  decreases with increasing train length, but is nearly independent of tunnel length and train speed in the usual range of  $R = 0.1-0.2$ , in agreement with full-scale tests (Peters 1990a).

## 4.2 Pressure Waves for Trains in Tunnels

As a train passes through a tunnel, a series of compression and expansion waves are formed that propagate along the tunnel at approximately the speed of sound. These waves cause a number of problems in the areas near the tunnel entrance and exit, both for the train and for the passengers. The limiting acceptable pressure change is known (Gawthorpe 1991) to be in the range of 1–4 kPa for a pulse length of 4–10 s, and modern train operations approach these limits. The pressure waves put a load on the structure of the cars and, as noted above, the pressure field affects the aerodynamic drag.

The pressure-time histories for an ICE train operating alone in a two-train tunnel, shown in Figure 10, can be used to illustrate a number of points. The pressure history is obviously the result of a very complicated wave pattern. Both full-scale and 1/25th-scale laboratory data using the facility shown in Figure 1 are included, and one can see that the data are in good agreement ( $\Delta p$  within 6%). Figure 11 shows typical results of a calculation that is discussed in more detail below, but it is helpful here to understand the main features of a complex flow of this type. Figure 11*a* shows an  $x$ - $t$  plot, and Figure 11*b* shows the pressure time history at a point  $\sim 20\%$  behind the train nose. Entering the tunnel, the nose of the train produces a compression wave, which is reflected from the tunnel exit as an expansion wave. As the tail of the train enters the tunnel, an expansion wave is produced that is reflected from the exit as a compression wave. In Figure 10, we see that the largest pressure pulse actually occurs in the middle of the tunnel (the location marked AB) as a result of a complex interaction between reflected nose and tail waves, the pressure variation on the nose, and the effects of friction on the sides of the train. Tunnel airshafts can be used to reduce the strength of the pressure pulses (Kim et al 1999).

Consider now the analysis of these flow phenomena. The problem is, in general, that of a three-dimensional, unsteady, turbulent, compressible flow, so analysis is rather daunting. However, some of the main features of these flows can be predicted well by idealized models (Howe 1999). Many workers use one-dimensional, unsteady, isentropic flow models (Matsuo et al 1997). A comparison between full-scale measurements and the idealized model for the pressure rise produced by the tunnel entry compression wave is shown in Figure 12.

The next level of analysis assumes a one-dimensional, unsteady, adiabatic, compressible flow, with wall friction effects on the train and tunnel wall that are modeled in the momentum equation with a quasi-steady assumption and work done by the train walls that is modeled in the energy equation. The resulting hyperbolic system of equations is solved by the method of characteristics. [See Sockel (1996) for a more detailed discussion.] The results presented in Figure 11 were obtained using this method. At the beginning of the process, the agreement of the pressure transients is, in general, very good. However, for longer times, the attenuation of the pressure waves is underestimated by the theory, possibly as a result of unsteady friction, the assumption of quasi-steady boundary conditions,

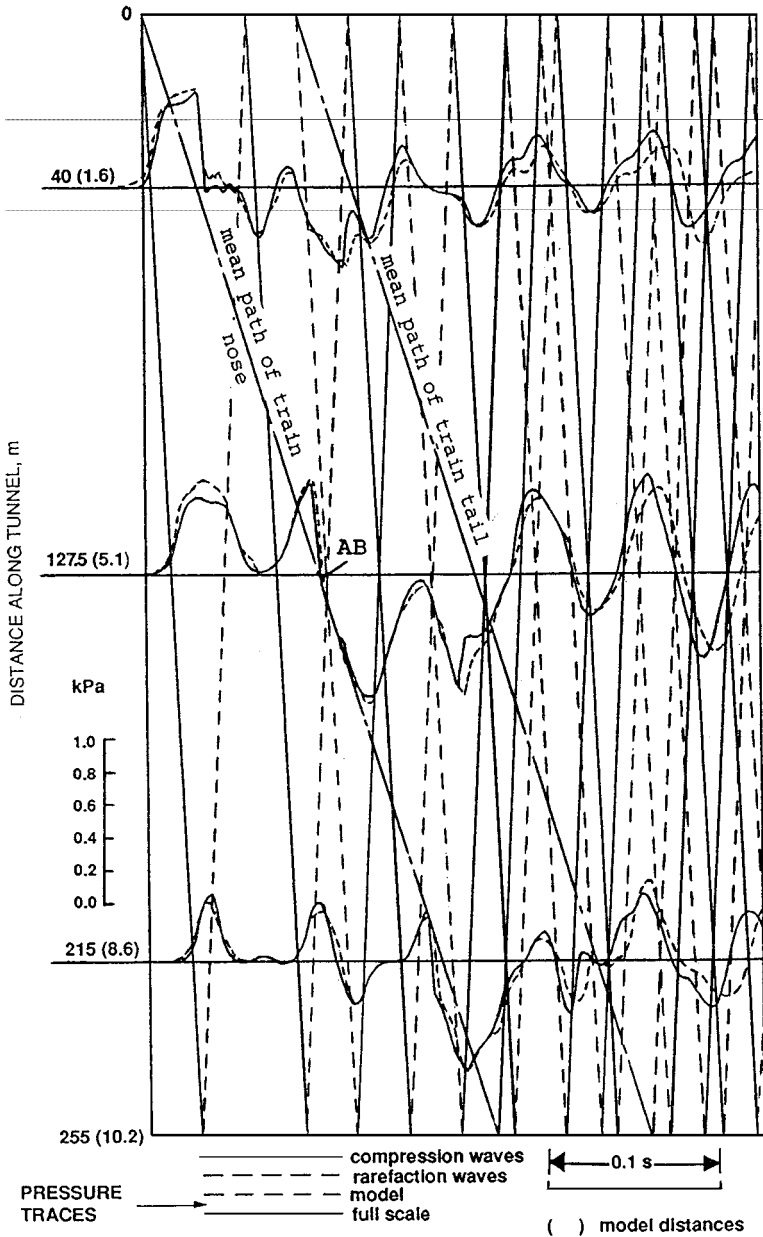


**Figure 10** Comparison of measurements at full-scale and 1/25th-scale for the pressure history of a train passing through a tunnel. (From Pope 1991, with permission of BHR Group Ltd.)

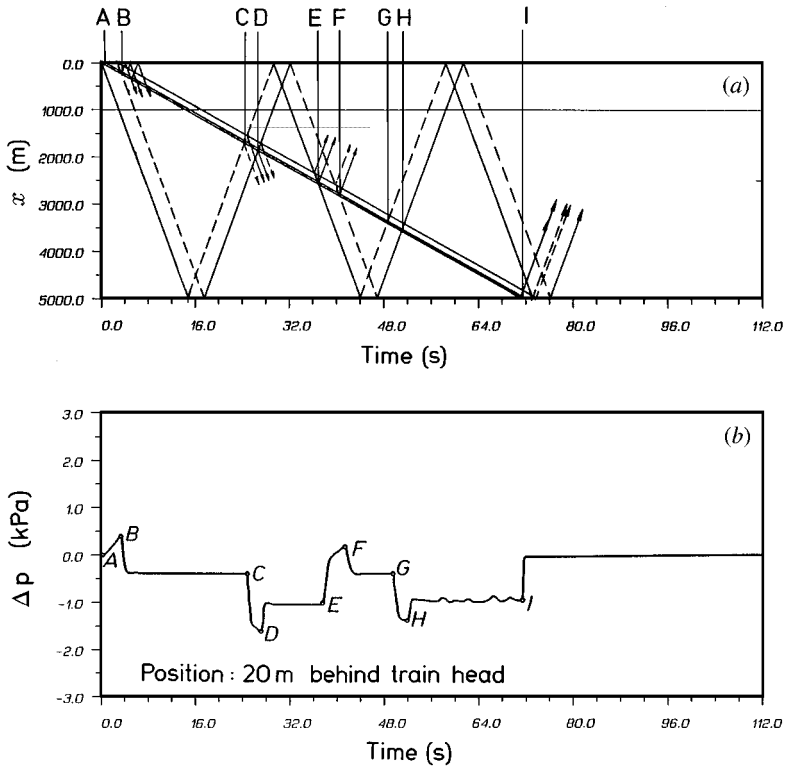


**Figure 11** Calculated pressure transients on a train passing through a tunnel. (a) Paths of train ends and propagation lines of waves, (b) pressure history at a point 20 m behind the nose,  $R = 0.363$ . (From Schulte & Sockel 1989, with permission of Addison Wesley Longman.)

the assumption of negligible heat transfer, and/or the porosity of the tunnel or train.

Several workers have applied the unsteady, three-dimensional Euler equations to train/tunnel problems (Gregoire et al 1997, Pahlke 1999a). Figure 13 shows favorable comparisons of pressure coefficient time histories from CFD predictions and model-scale experiments.

There have been a few very large scale RANS CFD studies of the unsteady flowfield generated along a high-speed train in a tunnel. Such flowfields can lead to troublesome vibrations. Suzuki (2000) used the marker and cell (MAC) method with the three-dimensional, unsteady, incompressible, RANS equations to study this process for Shinkansen trains operating both in a tunnel and in the open. He used 1.98 million grid points for the calculation in the open and 1.76 million grid points for the calculation in the tunnel. The predicted, instantaneous vorticity

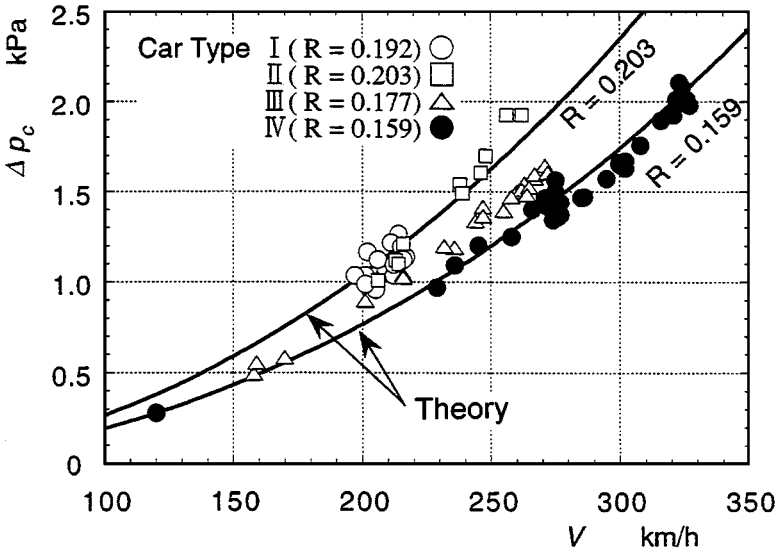


**Figure 12** Comparison of full-scale measurements and predictions with a simple, one-dimensional, unsteady model for the initial pressure rise as a train enters a tunnel. (From Matsuo et al 1997, with permission of BHR Group Ltd.)

pattern on the side of the train is shown in Figure 14, where one can see that the unsteadiness is more severe in the tunnel.

## 5. TRAINS PASSING TRACKSIDE STRUCTURES AND EACH OTHER

As an isolated train passes through the air, it induces a complicated flowfield. The implications of that flowfield on trackside structures and passing trains are much more important for trains than for other vehicles, because trains operate much closer to adjacent structures or other trains. Some of these implications are considered below.

### 5.1 Experimental Studies

A static pressure disturbance is caused first by the passing of the train nose and again by the passing of the tail. The magnitude of the pressure peak and the rate of the lateral decay are critical matters here, and some full-scale data from Tsuzuku et al (1999) are shown in Figure 15. It is clear that the effects of nose shape and cross-sectional area are very significant. The pressure peaks depend upon train speed squared. It is important to note that the rate of change is large (the timescale of the pulse scales well with the time required for the nose length of the train to

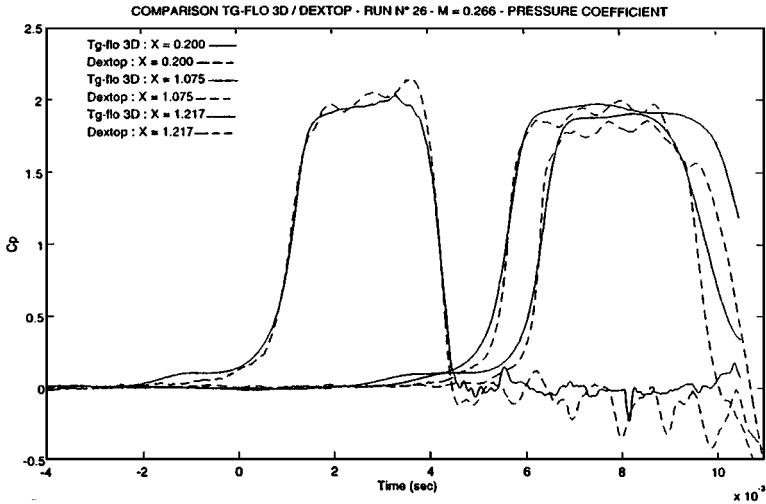
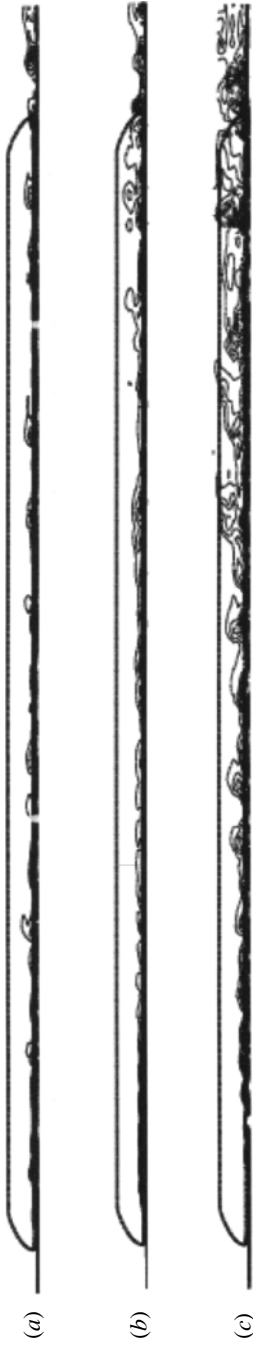


**Figure 13** Comparison of model-scale measurements and predictions with a numerical, three-dimensional, unsteady method using the Euler equations for the pressure transients as a train passes through a tunnel. (From Gregoire et al 1997, with permission of BHR Group Ltd.)

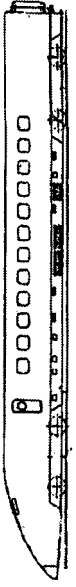
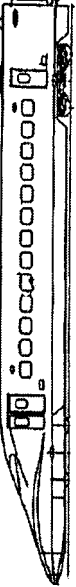
pass), which leads to impulsive loadings that can cause problems on such items as windows. These pressure phenomena can necessitate the installation of trackside noise barriers, which can reduce the pressure peaks by  $\sim 40\%$  at a train speed of 450 km/h (Tsuзuku et al 1999).

Wind forces in the slipstream can lead to serious trackside problems (Gawthorpe 1978). The high turbulence in the slipstream can endanger passengers on the platform, railway workers and carts, luggage, parcels, etc. The train flowfield is characterized by strong vorticity on the lee side, as discussed in section 3 above. This strongly nonuniform flowfield is aggravated further by unsteady effects caused by variations in the ambient wind. The gust associated with the train nose and the mean level of slipstream speed are reduced for the slender-nosed trains typical of modern high-speed designs compared to blunt-nosed shapes. However, the gusts in the wake are increased as a result of improved tail designs that cause narrower and more concentrated wakes. The slipstream speeds vary directly with train speed and depend very strongly on train shape. Penwarden (1974) considers that wind speeds  $> 20$  m/s are dangerous for people. Montagne (1973) measured forces on trackside cylinders that approximated people as TGV trains passed and found that the larger forces are produced by the passing of the tail up to a lateral distance of  $\sim 1.8$  m.

Next, consider a moving train passing another train, which may be at rest or moving in either the same or the opposite direction. The pressure pulses measured on the sides of passing trains depend strongly on train speed, nose shape, and



**Figure 14** Predicted vorticity patterns on the side of a Shinkansen train. (a) Train in the open, (b) train in a tunnel viewed from the tunnel center, (c) train in a tunnel viewed from the tunnel wall. (From Suzuki 2000, with permission of M Suzuki.)

Train series	Nose shape	Sectional View	Side view	Sectional area ( m <sup>2</sup> )	Nose length ( m )
300X	Roundwedge			9.1	6.0
	Cusp				
700	Aerostream			10.9	8.5
300	Slant			11.2	6.0

(a)

**Figure 15** Full-scale measurements of the pressure wave caused by the passage of a high-speed train. (a) Train shapes tested, (b) lateral decay of pressure. (From Tsuzuku et al 1999, with permission of Railroad Technical Research Institute.)

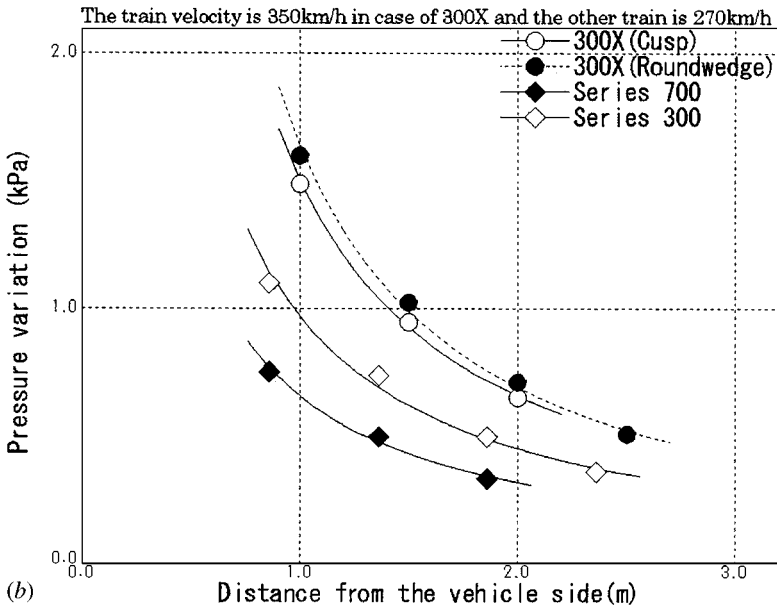


Figure 15 (continued)

separation distance, just as for trains passing trackside structures. The case of a streamlined, high-speed train passing a slower, conventional train with a bluff nose shape must also be considered. Studies of that situation are underway in the RAPIDE program (Schulte-Werning et al 1999a).

A recent set of full-scale data for high-speed trains can be found in Komatsu & Yamada (1999). Komatsu & Yamada instrumented a Shinkansen series 300 train (see Figure 15a) and measured pressure transients and lateral acceleration as the train passed similar trains and trains of other high-speed configurations at high relative speeds. Some results are presented in Figure 16. The peak positive and negative pressure excursions are given in nondimensional form as pressure coefficients, which are nearly constant as a function of train speed. Thus, the absolute pressure pulses vary as train speed squared. They are also a function of train nose shape. The lateral acceleration varies as train speed squared, and the absolute levels are quite substantial.

Much of the data in the literature was obtained at full scale, but model-scale testing of train passing is also common. The facility in Figure 1 is well suited to such studies, for example, and some recent work in that facility can be found in Johnson & Dalley (1999).

Now we come to the important matter of trains passing within the confines of a tunnel. This is a very complicated situation, because the train interaction now depends strongly on the relative times of entry of the two trains into the tunnel.

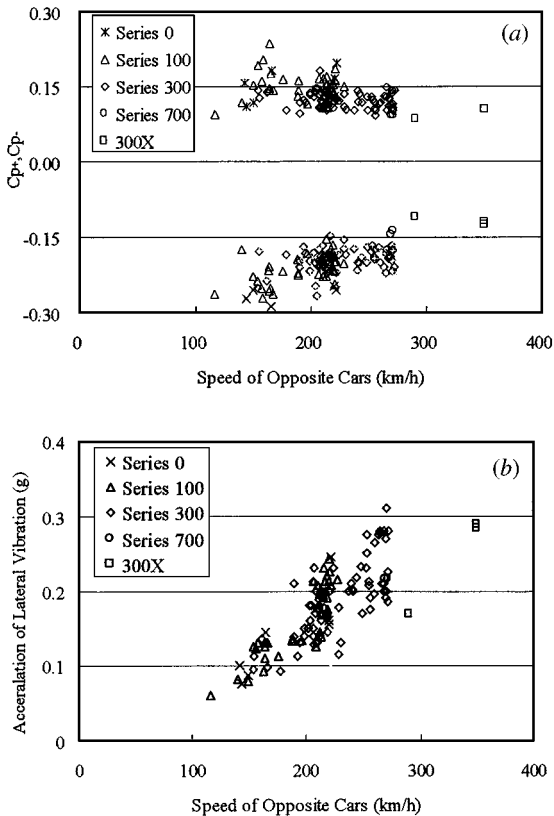


**Figure 16** Pressure pulses and lateral acceleration measured at full scale as a Shinkansen 300 series train passes trains of different configurations. (a) Peak pressure coefficients vs speed, (b) lateral acceleration vs speed. (From Komatsu & Yamada 1999, as presented at WCRR'99, with permission of Railroad Technical Research Institute.)

In one case, it was found that a shift in entry times of only 4 s could double the worst pressure change (Vardy & Anandarajah 1982). With all of the parameters and variables involved, it is not possible to select a sample of representative data for inclusion here. The model-scale tests of Johnson & Dalley (1999) with ETR 500 train models, in which one train was stationary near the tunnel entrance as the other passed, showed that the pressure pulse varied with train speed squared, nose shape, and track spacing. A long-nose design reduced the sensitivity to track spacing markedly. Full-scale data for two high-speed ETR 500 trains running in parallel in tunnels are available in Mancini & Violi (1999).

## 5.2 Analysis

Early analyses of the train-passing problem assumed incompressible, irrotational flow. These assumptions clearly become more restrictive as speed increases. Tollmien (1927) gives a two-dimensional, potential-flow solution for idealized trains passing in a tunnel.

Three-dimensional panel methods also have been applied to the situation of trains passing in a tunnel. Matschke et al (1999b) report good agreement between predictions using 4700 panels on each train, full-scale data, and model-scale data for a high-speed train passing a freight train. Matschke et al note that the best agreement was obtained for long nose shapes and wide track spacing, so that separation was avoided.

The next level of analyses involves numerical solutions of the three-dimensional Euler equations. Pahlke (1999b) contains a representative example of such treatments. Pahlke (1999b) provides a good discussion of the demands for accuracy and the practical issues involved in making calculations of this type for train-passing problems. For example, the pressure signals for a typical train-passing case in open air are only about  $\pm 10\%$  of the stagnation pressure, whereas transonic aircraft cases feature pressure changes on the order of 100% of the stagnation pressure. This leads to more restrictive gridding requirements. The level of agreement obtainable between predictions and full-scale data for ICE trains passing in the open at 250 km/h is illustrated in Figure 17 for surface pressure at particular locations on the train nose and tail. The peak values and time history are predicted quite well for the nose location, but are clearly overpredicted on the tail, and one might well attribute that to neglect of the influences of the thick boundary layers that develop along the trains.

CFD methods based on RANS have been applied to problems of high-speed trains passing in tunnels in a few cases. The severe gridding requirements that accompany unsteady, three-dimensional, high-Re turbulent flows have meant that rather coarse grids have been used even with advanced algorithms and advanced parallel-computing platforms. Some finite element method predictions of this class of methods can be found in Kalro & Tezduyar (1995). The pressure drop at the tail reaches a predicted maximum of 12 kPa, which is in approximate agreement with typical measured values of 14–16 kPa.

## 6. AERODYNAMIC NOISE

Noise is a very important environmental consideration both inside and outside of high-speed trains. Hardy (1999) provides a discussion of the situation from the point of view of the passenger. Noise problems as a result of pressure pulses caused by trains entering and exiting tunnels and passing trackside structures and other trains are discussed above. Iida et al (1999) discuss some methods for counteracting these problems. Aerodynamic noise also becomes significant at train speeds above 300 km/h. Aerodynamic noise level increases at about the sixth power of the train speed (Torii & Ito 1999). Measurement technology, analysis, and hardware studies of the aeroacoustics of high-speed trains are surveyed in King (1995)

Torii & Ito (1999) conducted full-scale studies of several sources of aerodynamic noise for Shinkansen trains. The change in nose shape shown in Figure 18 resulted in a 2-dB(A) reduction in noise measured 25 m from the track and also

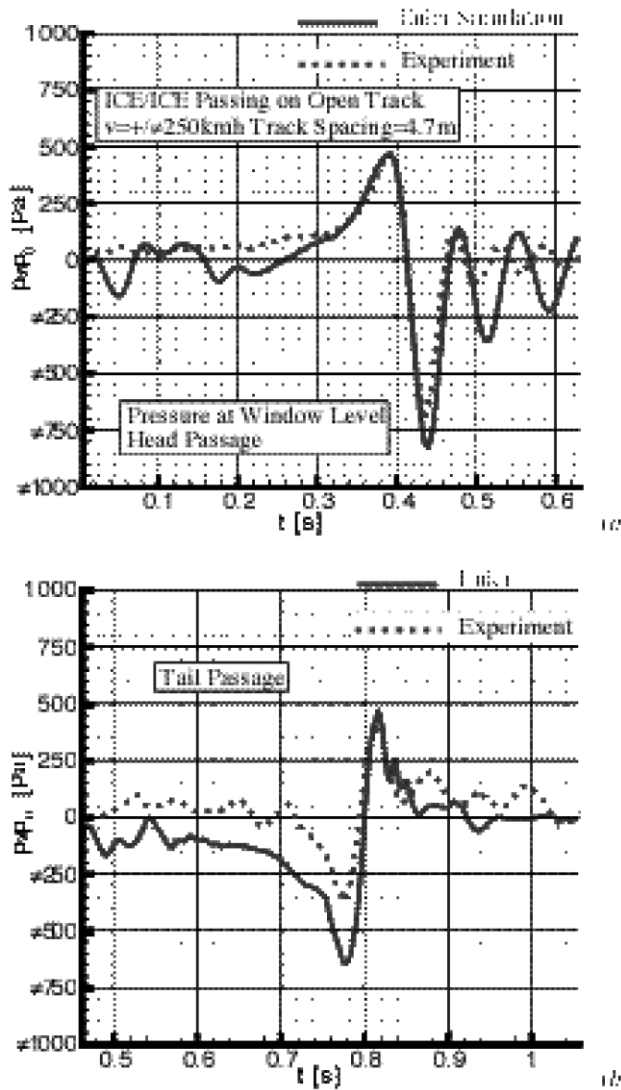


**Figure 17** Comparison of full-scale measurements and predictions with a numerical, three-dimensional, unsteady method using the Euler equations for the pressure transients as two InterCity Express trains pass at  $250 \text{ km h}^{-1}$ . (a) Nose passage, (b) tail passage. (From Pahlke 1999b, with permission of TRANSAERO Consortium.)

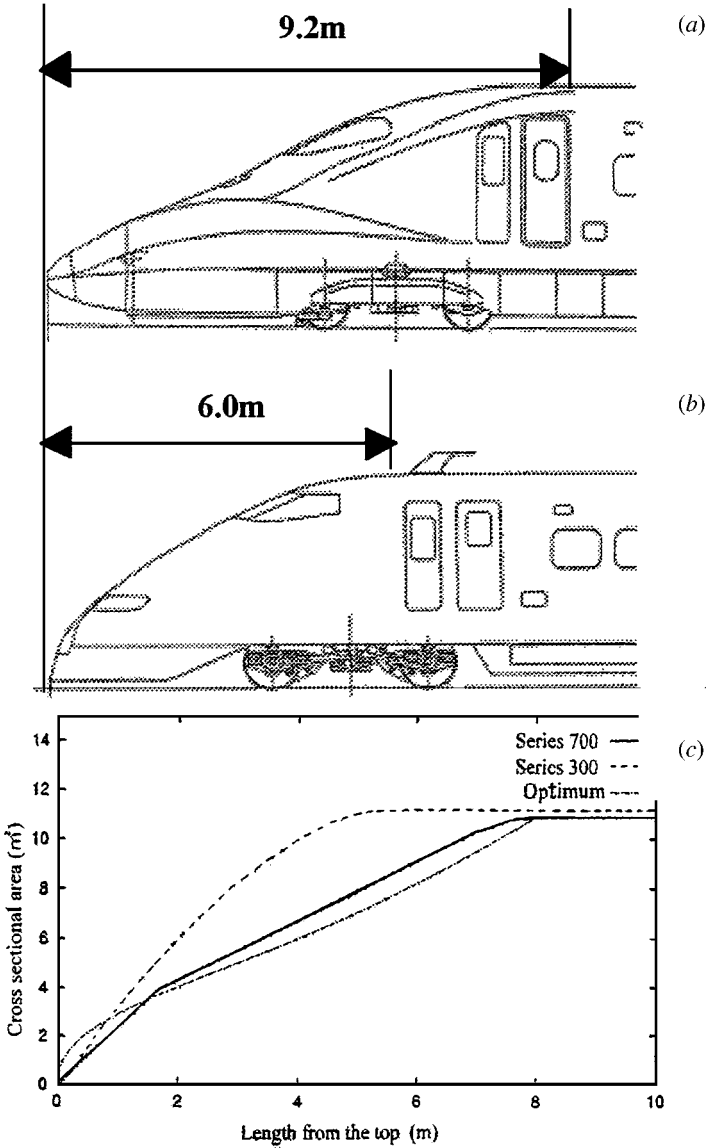


**Figure 18** Nose shapes studied to reduce aerodynamic noise and tunnel entry pressure pulses. (a) Shinkansen 700 series with lower noise, (b) Shinkansen 300 series, (c) cross-sectional area distributions. (From Torii & Ito 1999, as presented at WCRR'99, with permission of Railroad Technical Research Institute.)

reduced the pressure waves produced from tunnel entry. The shape change was accompanied by careful attention to roughness, the gaps and handles on the side doors, and aerodynamic treatments of the nose underbody. Takaishi et al (1999) used wind tunnel experiments at 1/12.5th scale and a two-dimensional, unsteady RANS CFD code to study aerodynamic noise sources from Shinkansen trains. They concluded that the mirror-image method with two models was more useful for studying such flows than a single model on a moving ground plane.

Talotte et al (1999) describe a combined experimental/computational study of aerodynamic noise generated by car irregularities. The experiments were conducted in an anechoic wind tunnel using models of idealized irregularities. The aeroacoustic computations use a method coupling large eddy simulations (LES) of the unsteady turbulent flow and linearized Euler equations for the acoustic propagation.

Intensive studies of the effects of bogie fairings on drag and aerodynamic noise are ongoing (Schulte-Werning et al 1999b).

The pantograph continues to receive attention as a source of aerodynamic noise as well as drag and lift (Torii & Ito 1999, Althammer et al 1999, Ikeda 1999). Torii & Ito (1999) achieved a 4-dB(A) reduction in noise caused by the pantograph on full-scale measurements of the Shinkansen 700 series train compared with the 300 series. Althammer et al (1999) report noise reductions as large as 13–16 dB(A) in wind tunnel tests of innovative pantograph configurations; however, large lift forces were encountered. Ikeda (1999) presents a low-noise pantograph design that overcame that problem.

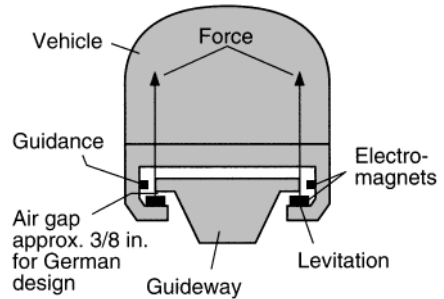
## 7. AERODYNAMICS OF MAGNETIC LEVITATION TRAINS

A number of concepts have been advanced to replace the conventional wheel-on-track support and propulsion system for higher-speed trains. The Aerotraine (Guienne 1972) used jet engines for propulsion and an air cushion for suspension. Various arrangements have also been suggested for high-speed trains that operate continuously in tubes (Hammit 1972) with different types of propulsion systems, including simple air-pressure differences. More recently, attention has been focused almost exclusively on magnetic levitation (Maglev) and propulsion systems.

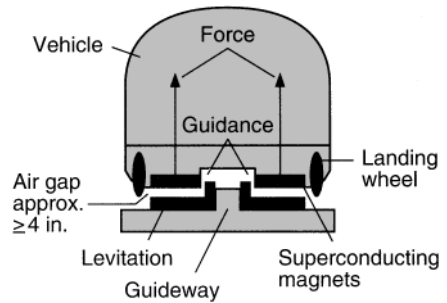
The notion of using magnetic levitation and/or propulsion for trains dates back many years. A historical overview of the topic up until the early 1990s can be found in Stix (1992). For a number of practical reasons, Maglev systems usually involve trains moving over an elevated track on the order of tens of meters above the ground. There are two general arrangements for using the magnetic forces, and the aerodynamic issues involved in each are quite different. The electromagnetic suspension (EMS) arrangements have a T-shaped track, and the lower part of the Maglev vehicle is wrapped around the track (see Figure 19a). Attractive magnets

**Figure 19** Schematics of EMS and EDS for Maglev trains.

**Electromagnetic maglev system (EMS)**



**Electrodynamic maglev system (EDS)**



are located on the bottom of the track and on the portion of the vehicle that wraps around the track, and the clearance between the vehicle and the bottom of the track is on the order of a centimeter. The TRANSRAPID system in Germany is of this EMS type. In the electrodynamic suspension (EDS) arrangement shown in Figure 19b, the vehicle rides above the track, often in a rectangular or U-shaped trough, with repulsive magnets on the track and the bottom of the vehicle. The gaps between the vehicle and the track are much larger, approximately 10 cm, for these configurations. The current Japanese systems are of this EDS type and use a rectangular trough. If a shallow U-shaped trough arrangement is used, the aerodynamicist must obviously pay careful attention to lift and side forces so that the vehicle remains above the track. Indeed, the generation of lift by the body is viewed as undesirable for both types of Maglev systems, because lift varies so strongly with vehicle speed. The designers much prefer to generate all the forces needed for levitation by the magnets.

## 7.1 Experimental Studies

Peters (1983) provides a good overview of wind tunnel studies of the aerodynamics of early EMS vehicle configurations. The area between the bogies and the track requires attention, or the drag from the bogies can be two thirds of the drag of the whole vehicle (Peters 1983). However, careful design of the bogies and fairings

has reduced this source of drag by a factor of 2. Peters (1983) also reports that the narrow gaps between the track and the underbody can reduce the frictional drag in that area by 50%, based on towing-tank tests. The influence of the nose and tail on the overall drag of the vehicle is generally larger for Maglev trains than for conventional trains, because current Maglev arrangements are much shorter. Nose and tail shapes with slenderness ratios of 1.25 that have proven efficient for wheel/rail trains were also found to be applicable for Maglev vehicles so long as sharp edges are avoided. Model-scale drag results, including the effects of crosswinds, are given in Figure 20. With no crosswind (zero yaw angle), the drag of a two-car vehicle is about equally divided between the leading and trailing cars. As yaw angle increases, the drag of the leading car decreases and that of the trailing car increases in the same manner as the nose and tail drag. The drag of the whole vehicle increases in a nearly linear fashion. Peters (1983) states that the drag deduced from full-scale coasting tests is in agreement with that from the wind tunnel tests.

Side-force and lift data are presented in Figure 21. The side force on the leading car is much larger than that on the trailing car, and most of the side force on the leading car comes from the nose. The lift on the nose changes little with yaw angle, but the lift on the whole vehicle increases sharply with increasing yaw. The lift was reduced by the addition of an air deflector under the nose.

A special apparatus with a high-speed (150 mph) moving belt to simulate a Maglev train traveling over an elevated track was installed in the  $6 \times 6 \times 24$ -ft

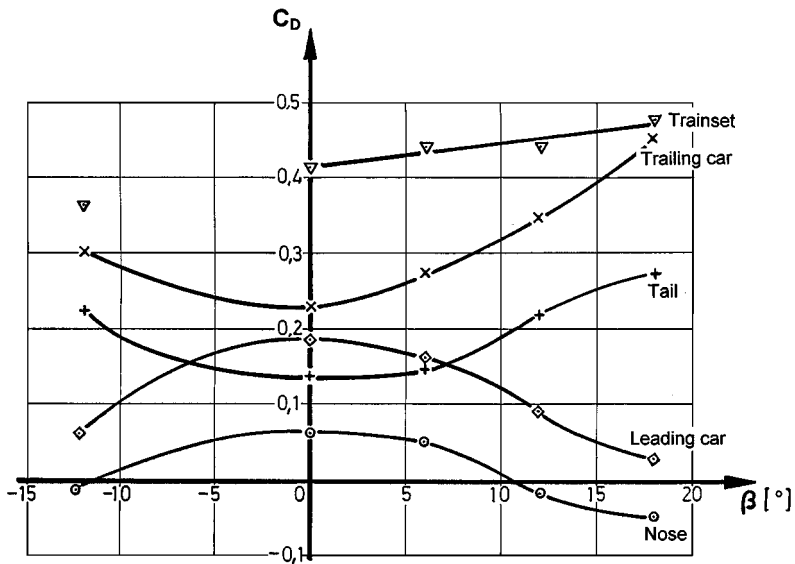


**Figure 20** Variation of drag coefficient with yaw angle for a 1/10th-scale electromagnetic suspension system (EMS) Maglev model showing the contribution of each car and the extremities. (From Peters 1983, with permission of Inderscience Enterprises Ltd.)

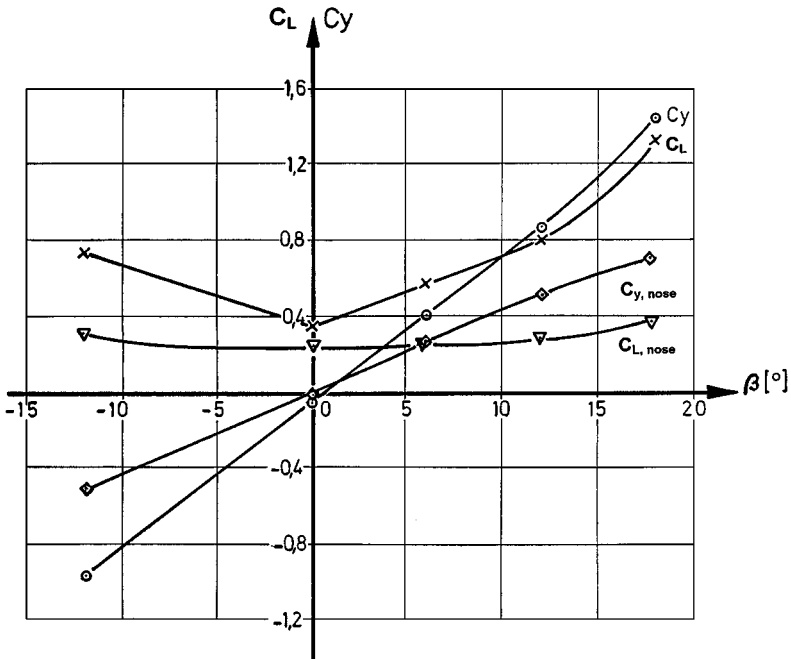
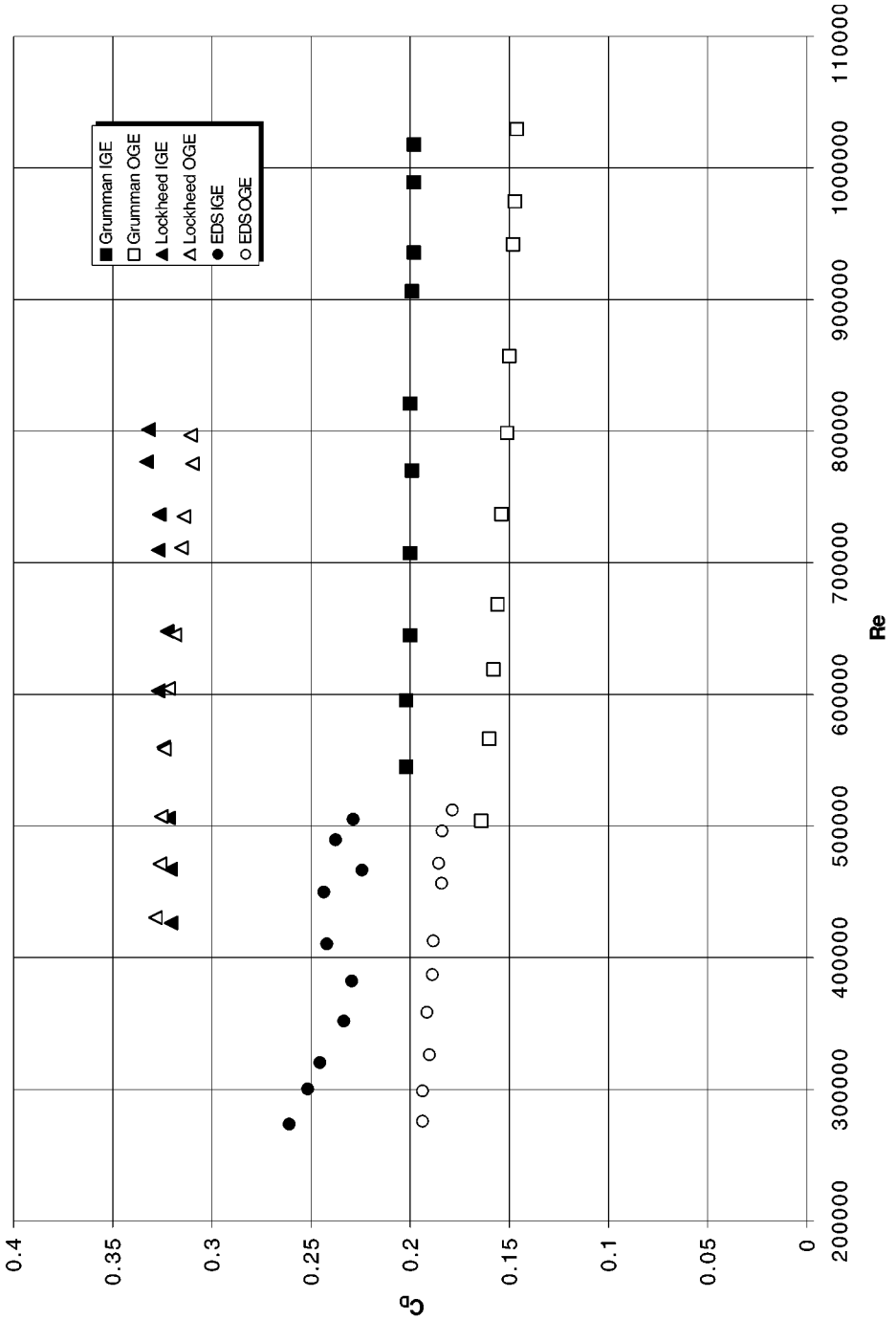


**Figure 21** Variation of lift and side-force coefficients with yaw angle for the leading car of the TRANSRAPID TR06 Maglev train. (From Peters 1983, with permission of Inderscience Enterprises Ltd.)

wind tunnel at Virginia Polytechnic Institute and State University (Virginia Tech) (Tyll et al 1996a). Howell (1986) had shown that testing above a fixed track in a wind tunnel did not simulate the flow under a Maglev vehicle accurately. The apparatus is shown in Figure 22 in the wind tunnel with an EMS vehicle model mounted over and around the moving belt. A large fairing can be seen mounted in front of the support and the front pulley driving the moving belt. The shape of this fairing resulted from intensive studies of the flowfield over and around the sides of the moving belt. The goal was to minimize any inviscid and turbulent disturbances caused by the elevated moving belt (which simulated the elevated track) to the desired uniform, turbulence-free flow approaching the

**Figure 23** Wind tunnel drag coefficient data for a Grumman electromagnetic suspension system (EMS) Maglev vehicle design, a Lockheed electrodynamic suspension system (EDS) Maglev vehicle design, and a Virginia Tech electrodynamic suspension system (EDS) Maglev vehicle design, all operating on a track [i.e. in-ground effects (IGE)] and without a track [i.e. out-of-ground effects (OGE)].  $C_D$ , drag coefficient; Re, Reynolds number. Data taken from Tyll et al (1996a), Liu et al (1996), Pulliam et al (1996), and Wilt et al (1997).



Maglev models. This effort was ultimately successful, and the resulting quite uniform flowfield measured without a model over the belt is documented in Tyll et al (1996a). This facility has been used to perform studies of the aerodynamics of several rather different Maglev vehicles (Tyll et al 1996a, Liu et al 1996, Pulliam et al 1996, Wilt et al 1997). There were two streamlined EMS designs from Grumman (one can be seen in Figure 22): a blunt EDS design produced by Lockheed for American Maglev Technology, in which the suspension system featured narrow, vertical blades projecting up into the vehicle; and a streamlined EDS design developed at Virginia Tech to operate in a shallow U-shaped trough. It was a challenge to force the moving belt into the shape of a shallow trough while operating at high speeds. The data include force and moment coefficients, skin friction measurements in the gaps between the vehicles and tracks, mean-flow and turbulence velocity surveys, and surface flow visualizations with tufts.

Drag and lift comparisons are presented here in Figures 23 and 24, in which the IGE and OGE notations refer to “in-ground effect” and “out-of-ground effect” (i.e. with the moving belt in place or not), respectively. First, it can be seen that above an  $Re$  based on model width of  $\sim 400,000$ , the  $Re$  dependence essentially disappears. Second, for the streamlined shapes, there is an increase in drag and a change in lift when the vehicle is operating near the track. The blunt shape shows an increase in lift, but very small changes in drag. The streamlined shapes show good drag levels and workable levels of lift, whereas the blunt shape shows high drag and high lift, both of which are undesirable for Maglev vehicles from an aerodynamics point of view.

A sample of wake survey data for the Grumman design is shown in Figure 25. That data is used for comparison with CFD predictions below.

The Yamanashi Maglev test line in Japan is producing a great deal of useful full-scale data on all aspects of Maglev vehicle operation, including aerodynamics (Suzuki et al 1999). The current designs are of the EDS type, with the vehicle operating in a rectangular trough with sides reaching up to about half the height of the vehicle. The nose shapes have been carefully designed, based on extensive CFD studies (described below), to minimize aerodynamic noise and drag and pressure pulses when operating through tunnels. There are two shapes currently under test. One nose has a long, slightly rounded wedge shape (called the aerowedge), and the other has a shape like a duck’s bill (also called the double-cusp). Much of the current testing is focused on vertical, lateral, and rolling-vehicle stability at low and high speeds, including running in a turn in a curved track section and passing

---

**Figure 24** Wind tunnel lift coefficient data for a Grumman electromagnetic suspension system (EMS) Maglev vehicle design, a Lockheed electrodynamic suspension system (EDS) Maglev vehicle design, and a Virginia Tech electrodynamic suspension system (EDS) Maglev vehicle design, all operating on a track [i.e. in-ground effects (IGE)] and without a track [i.e. out-of-ground effects (OGE).]  $C_L$ , lift coefficient;  $Re$ , Reynolds number. Data taken from Tyll et al (1996a), Liu et al (1996), Pulliam et al (1996), and Wilt et al (1997).

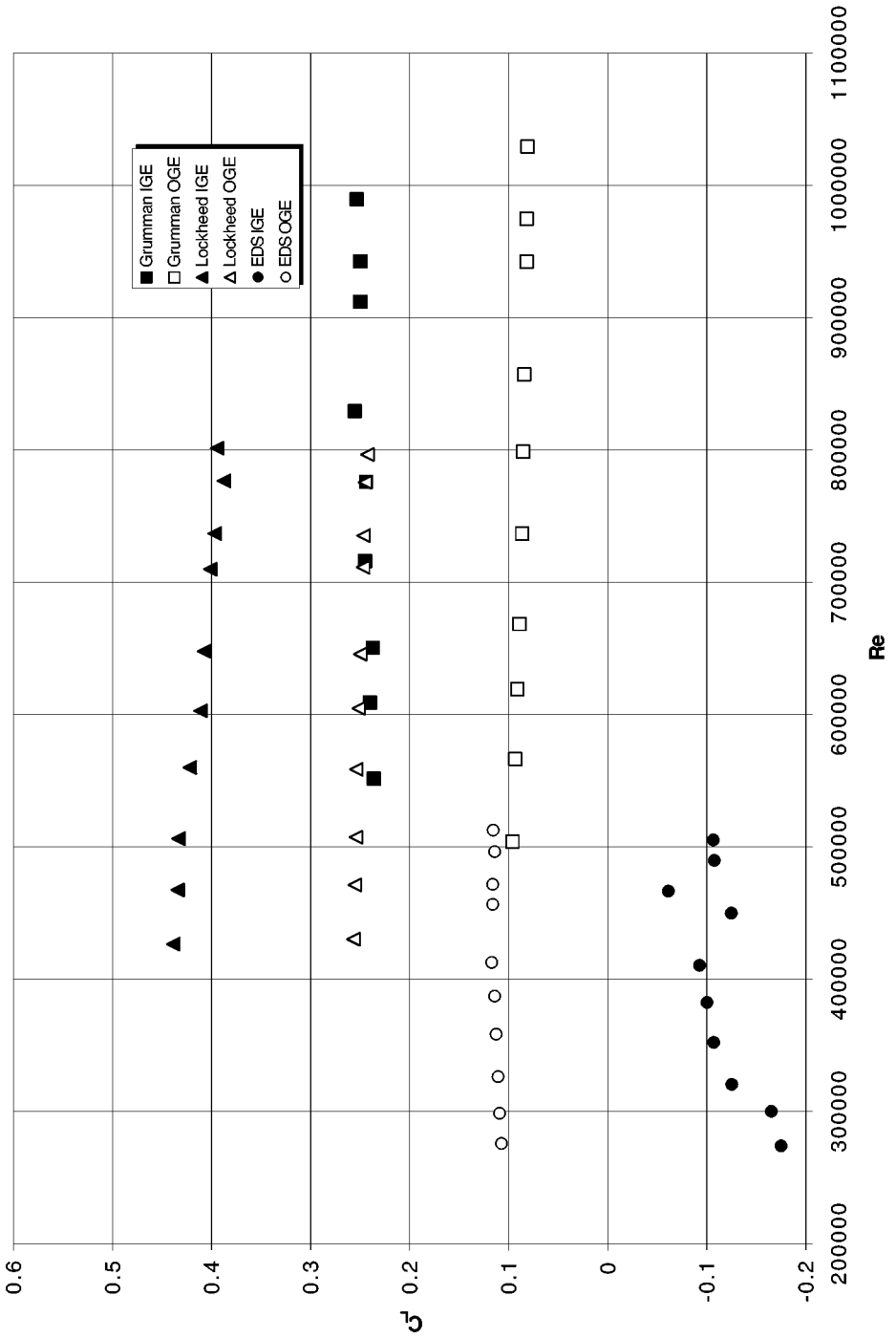
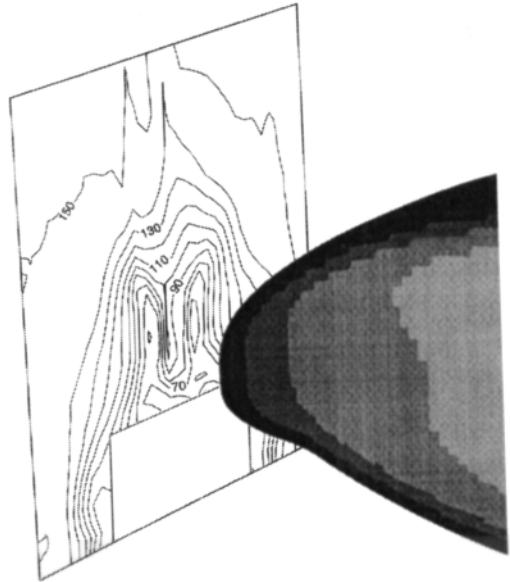


**Figure 25** Velocity contours on a cross-plane in the wake behind the Grumman Maglev vehicle design in the Virginia Tech wind tunnel. (From Tyll et al 1996a, with permission of the American Institute of Aeronautics and Astronautics.)



other trains. Tests have been run up to speeds of 550 km/h, and train-passing tests have been run up to relative speeds of 966 km/h. The aerodynamic lift is about 50 kiloNewtons (kN) at 500 km/h, and there is little difference between operations in the open or in a tunnel. Lateral and vertical displacement excursions were on the order of  $\pm 10$  mm for runs up to 500 km/h on both straight- and curved-track sections. Side forces experienced in passing events were larger than vertical forces or rolling moments, and the effects were similar to those observed for conventional trains. Yoshimura et al (1999) report results of tests of different aerodynamic braking systems, which they found to be quite effective because of the high speed of the Maglev vehicles.

## 7.2 Analysis

Early analyses of the aerodynamics of Maglev trains followed closely the methods used for conventional trains, as described in Section 2.2 above. Barrows et al (1992) attempted to model the effects of vortex shedding for an EDS vehicle in a rectangular trough by modeling the flow as a point source located between two parallel plates. The kinetic energy in the flow was then related to a drag caused by vortex shedding, and an optimum nose shape was predicted.

Maglev vehicles all operate very close to the track or ground, with the EMS systems being the closest. Thus viscous effects between the vehicle and the track can be expected to be important, and low-order, inviscid, panel methods will suffer from their inability to model such important phenomena as “lift reversal,”

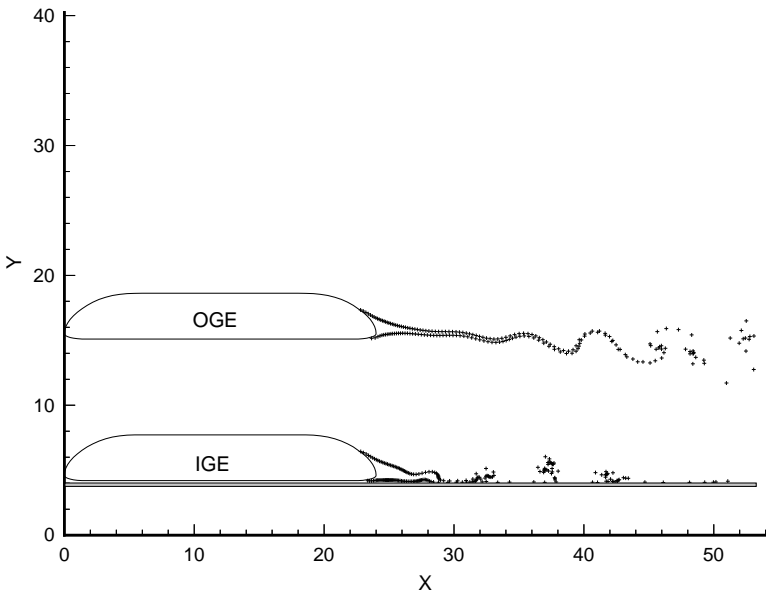


**Figure 26** Vortex panel method solution for flow over the Grumman Maglev design. Here OGE denotes “out of ground effect,” and IGE denotes “in ground effect.” (From Tyll et al 1998, with permission of the authors.)

which occur when a vehicle operates in close proximity to the ground or a track. On the other hand, there is a need for relatively simple and inexpensive analyses for such purposes as multidisciplinary design and optimization (MDO) studies.

Tyll et al (1998) found that the vortex panel method was a low-order method capable of simulating many of the important viscous effects without going to the complexity of a RANS CFD treatment. Figure 26 shows the vortical flow patterns predicted for a two-dimensional version of the Grumman Maglev vehicle design in which the in-ground and out-of-ground effects are denoted. Figure 27 shows a comparison of the pressure distribution over and under the same two-dimensional body in-ground effect as predicted by the vortex panel method and a two-dimensional RANS CFD calculation from Siclari et al (1995). Rather good agreement can be seen. Especially noteworthy is the correct shape of the pressure distribution under the vehicle from the vortex panel method, which cannot be predicted by inviscid, low-order methods. Based on this success, the vortex panel method was integrated into an multidisciplinary design and optimization code for Maglev vehicle shape design (Tyll et al 1996b, Tyll & Schetz 1998). The method proved capable of predicting minimum drag shapes quite close to those resulting from RANS CFD studies, described below. Indeed, one design from the multidisciplinary design and optimization code closely resembles the nose shape,

with a protruding lower lip that was recently adopted for the latest Shinkansen trains.

As just noted above, the selection of the nose shape for Maglev trains has been the subject of extensive RANS CFD studies, combined with wind tunnel and sometimes full-scale tests. The duck's bill or double-cusp shape and the aerowedge shapes mentioned above were both designed in this way (Miyakawa & Hosaka 1993, Takao et al 1993). Predictions of the flow over the double-cusp design operating in the rectangular trough are given in Figure 28.

Siclari et al (1993, 1995) used RANS CFD methods to arrive at the EMS Maglev vehicle designs that were later tested in the wind tunnel at Virginia Tech. The flowfield predicted at the tail of the body, as shown in Figure 29, was in good agreement with that observed in the wind tunnel (Tyll et al 1996a).

Klopfer & Mehta (1995) applied RANS CFD techniques to an EDS Maglev vehicle design that was intended to operate in a shallow U-shaped trough. Figure 30 displays predictions of the flow over and around the body and trough, showing the vortex pattern in the wake behind the truncated tail.

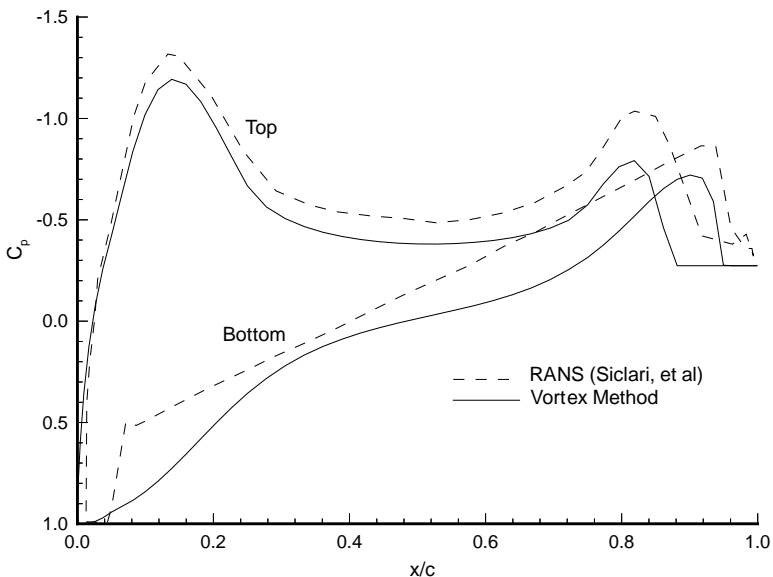


**Figure 27** Comparison of Reynolds-averaged Navier-Stokes computational fluid dynamic solution from Siclari et al (1995) and vortex panel method solutions for pressure distribution over the Grumman Maglev design in ground effect. (From Tyll et al 1998, with permission of the authors.)

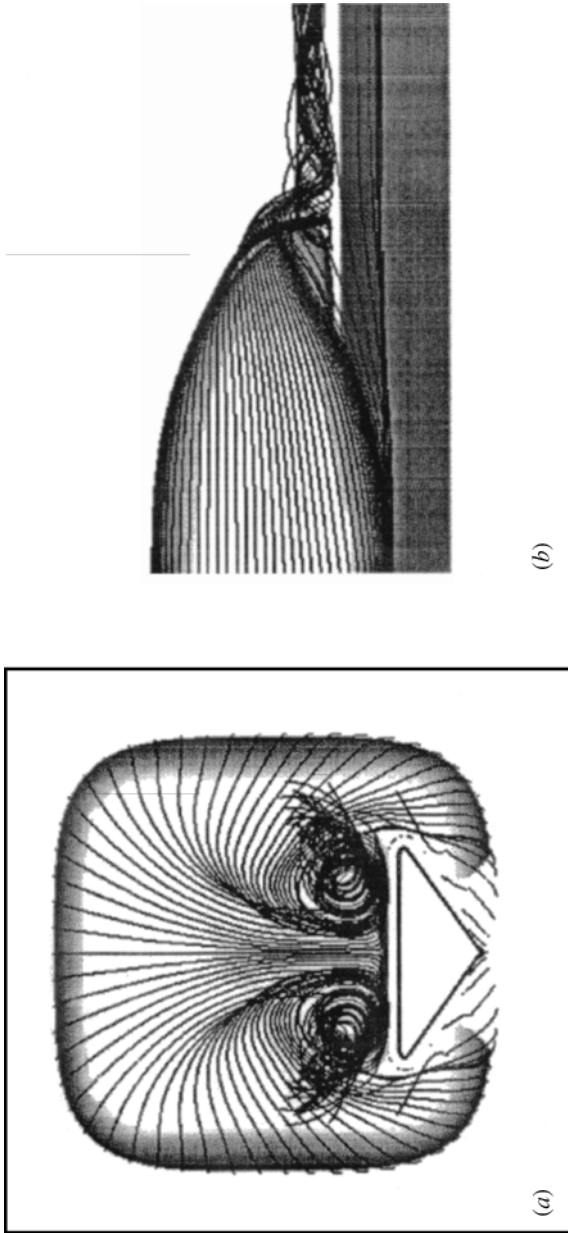


**Figure 29** Reynolds-averaged Navier-Stokes computational fluid dynamic solution for the flow over the tail of the Grumman Maglev design on an elevated track. (a) View looking upstream from the rear. (b) View looking at the tail from the side. (From Siclari et al 1995, with permission of the American Institute of Aeronautics and Astronautics.)

Visit the Annual Reviews home page at [www.AnnualReviews.org](http://www.AnnualReviews.org)

## LITERATURE CITED

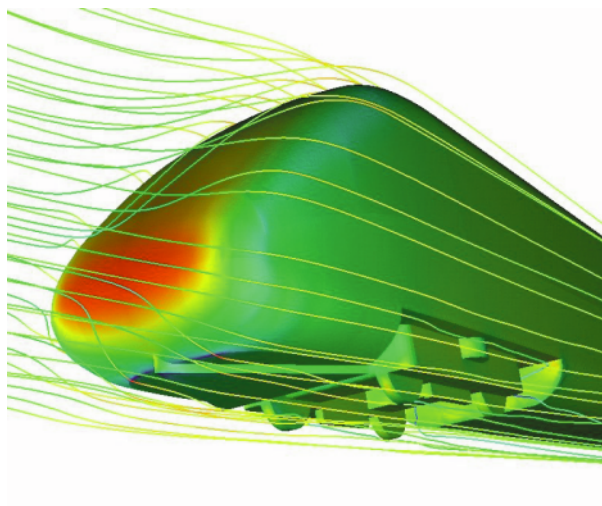
- Althammer K, Baldauf W, Lölgen T. 1999. Considerations for high performance pantographs. *Proc. World Congr. Railw. Res., Tokyo*: Tokyo: Railr. Tech. Res. Inst. (CD-Rom)
- Baker CJ. 2000. The wind tunnel determination of crosswind forces and moments on a high speed train. In *Proc. Brite/Euram Proj. Symp. Transient Aerodyn. Railw. Syst. Optim., Paris, 1999*, ed. B Schulte-Werning, R Gregoire, A Malfatti, G Matschke. Wiesbaden, Ger.: Verlag Vieweg. In press
- Baker CJ, Brockie NJ. 1991. Wind tunnel tests to obtain aerodynamic drag coefficients: Reynolds number and ground simulation effects. *J. Wind Eng. Ind. Aerodyn.* 38:23–28
- Baker CJ, Humphreys ND. 1991. *Aerodynamic forces and moments on containers on flat wagons in cross winds from moving model test. FR 91017*. Dep. Civ. Eng. Nottingham Univ. Nottingham, UK
- Baker CJ, Humphreys ND. 1996. Assessment of the adequacy of various wind tunnel techniques to obtain aerodynamic data for ground vehicles in cross winds. *J. Wind Eng. Ind. Aerodyn.* 60:49–68
- Baker CJ, Wright NG, Johnson, Gaylard AP. 1999. *Inland Surface Transport LINK Scheme. Final Proj. Rep.*, Univ. Birmingham. Birmingham, UK
- Barrows T, McCallum D, Mark S, Castellino RC. 1992. *Aerodynamic Forces on Maglev Vehicles. DOT/FRA/NMI-92/21*. US Dep. Transp. Washington, DC
- Bearman PW, Mullarkey SP. 1994. Aerodynamic forces on road vehicles due to steady side winds and gusts. In *Proc. RAeS Conf. Veh. Aerodyn., Loughborough*. London, UK: R. Aeronaut. Soc. London
- Bernard M. 1973. La soufflerie à veine longue de l'Institut Aérotechnique de SainCyr-L'Ecole. *Rev. Gén.Chemins Fer.* January
- Bernard M, Guiheu C. 1976. Mesures recentes de la resistance a l'avancement de materi- als roulant. *Rev. Gén. Chemins Fer., April*, pp. 243–55
- Brockie NJ, Baker CJ. 1990. The aerodynamic drag of high speed trains. *J. Wind Eng. Ind. Aerodyn.* 34:273–90
- Chiu TW. 1995. Prediction of the aerodynamic loads on a railway train in a cross-wind at large yaw angles using an integrated two- and three-dimensional source/vortex panel method. *J. Wind Eng. Ind. Aerodyn.* 57:19–39
- Chiu TW, Squire LC. 1992. An experimental study of the flow over a train in a crosswind at large yaw angles up to 90°. *J. Wind Eng. Ind. Aerodyn.* 45:47–74
- Cooper RK. 1984. Atmospheric turbulence with respect to moving ground vehicles. *J. Wind Eng. Ind. Aerodyn.* 17:215–38
- Copley C. 1987. The three-dimensional flow around railway trains. *J. Wind Eng. Ind. Aerodyn.* 26:21–52
- de Wolf WB, Demmenie EAFA. 1997. A new test facility for the study of interacting pressure waves and their reduction in tunnels for high-speed trains. In *Proc. Int. Symp. Aerodyn. Vent. Veh. Tunn., 9th, Aosta Valley, Italy*. London: ME Publ.
- Dominy RG, Docton MKR. 1994. Passenger vehicles in unsteady cross winds. In *Proc. RAeS Conf. Veh. Aerodyn., Loughborough*. London, UK: R. Aeronaut. Soc. London
- Gaillard MA. 1979. Aerodynamic measurements with high-speed trains (250 km/h) in the Heitersburg tunnel. In *Proc. Int. Symp. Aerodyn. Vent. Veh. Tunn., 3rd, Sheffield, UK*, pp. 343–62. Cranfield, UK: BHRA Fluid Eng. Cent.
- Gawthorpe RG. 1978. Aerodynamics in railway engineering. 1. Aerodynamics of trains in the open air. *Proc. World Congr. Inst. Mech. Eng. Railw. Eng. Int.*, pp. 7–12
- Gawthorpe RG. 1983. Train drag reduction from simple design changes. In *Impact of*

- Aerodynamics on Vehicle Design*, ed. MA Dorgham, pp. 308–41. London: Inderscience
- Gawthorpe RG. 1991. Pressure comfort criteria for rail tunnels operations. In *Aerodynamics and Ventilation of Vehicle Tunnels*, ed. A Haerter, pp. 173–88. New York: Elsevier
- Gawthorpe RG. 1994. Wind effects on ground transportation. *J. Wind Eng. Ind. Aerodyn.* 52(1–3):73–92
- Gawthorpe RG, Pope CW, Green RH. 1979. Analysis of train drag in various configurations of a long tunnel. In *Proc. Int. Symp. Aerodyn. Vent. Veh. Tunn., 3rd, Sheffield, UK*. Pap. C1. Cranfield, UK: BHRA Fluid Eng.
- Gaylard AP. 1993. The application of computational fluid dynamics to railway aerodynamics. *Proc. World Congr. Inst. Mech. Eng.* 207:133–41
- Grégoire R, Réty JM, Masbernat F, Morinère V, Bellenoue M, Kageyama T. 1997. Experimental study (scale 1/70th) and numerical simulations of the generation of pressure waves and micro-pressure waves due to high-speed train-tunnel entry. In *Proc. Int. Symp. Aerodyn. Vent. Veh. Tunn., 9th, Aosta Valley, Italy*. London: ME Publ.
- Guienne P. 1972. High speeds and Aerotrain. In *High Speed Ground Vehicles. VKI Lect. Ser.* Brussels, Belg.: von Karman Inst.
- Guiheu C. 1982. La résistance a l'avancement des rames TGV-PSE. *Rev. Gén. Chemins Fer*. January
- Hammitt AG. 1972. High speed tube vehicle systems. In *High Speed Ground Vehicles. VKI Lect. Ser. 48*. Brussels, Belg.: von Karman Inst.
- Hardy AEJ. 1999. Railway passengers and noise. *Proc. World Congr. Inst. Mech. Eng.* 213F:173–80
- Heine C, Matschke G. 2000. Full scale tests on side wind effects on trains: evaluation of aerodynamic coefficients and efficiency of wind breaking devices. In *Proc. Brite/Euram Proj. Symp. Transient Aerodyn. Railw. Syst. Optim., Paris, 1999*, ed. B Schulte-Werning, R Gregoire, A Malfatti, G Matschke. Wiesbaden, Ger.: Verlag Vieweg. In press
- Howe MS. 1999. Review of the theory of the compression wave generated when a high-speed train enters a tunnel. *Proc. World Congr. Inst. Mech. Eng.* 213F:89–104
- Howell JP. 1986. Aerodynamic response of Maglev train models to a crosswind gust. *J. Wind Eng. Ind. Aerodyn.* 22:205–13
- Iida M, Fukuda T, Kikuchi K, Murata K, Yamauchi N. 1999. Infrasound problems near tunnel portals of high-speed railway. In *Proc. World Congr. Railw. Res., Tokyo*. Tokyo: Railr. Tech. Res. Inst. (CD-Rom)
- Ikeda M. 1999. Passive lift suppression mechanism for low noise pantograph. In *Proc. World Congr. Railw. Res., Tokyo*. Tokyo: Railr. Tech. Res. Inst. (CD-Rom)
- Johnson T, Dalley S. 1999. 1/25 scale moving model tests for the TRANAERO project. In *Proc. Brite/Euram Proj. Symp. Transient Aerodyn. Railw. Syst. Optim., Paris, 1999*, ed. B Schulte-Werning, R Gregoire, A Malfatti, G Matschke. Wiesbaden, Ger.: Verlag Vieweg. In press
- Karlo V, Tezduyar TE. 1995. Parallel finite element computation of 3D incompressible flows. In *Solution Techniques for Large-scale CFD Problems*, ed. WG Habashi, pp. 1–23. New York: Wiley & Sons
- Kim D-H, Min D, Oh I-G. 1999. Experimental study of the aerodynamic countermeasures for reducing the micro-pressure waves and pressure fluctuations in high-speed train-tunnel interfaces. In *Proc. World Congr. Railw. Res., Tokyo*. Tokyo: Railr. Tech. Res. Inst. (CD-Rom)
- King WF III. 1996. A précis of developments in the aeroacoustics of fast trains. *J. Sound Vib.* 193(1):349–58
- Klopfer GH, Mehta UB. 1995. *Aerodynamic Computations for High-Speed, Magnetic-Flight System. AIAA 95-0749*. New York: Am. Inst. Aeronaut. Astronaut.
- Komatsu N, Yamada F. 1999. The reduction of the train draft pressure in passing by each other. In *Proc. World Congr. Railw. Res.,*

- Tokyo. Tokyo: Railr. Tech. Res. Inst. (CD-Rom)
- Krönke I, Sockel H. 1994. Model tests about cross wind effects on containers and wagons in atmospheric boundary layers. *J. Wind Eng. Ind. Aerodyn.* 52:109–19
- Liu D, Marshakov A, Marchman JF III, Schetz JA. 1996. *Aerodynamic Evaluation of Two Maglev Vehicle Designs*. SAE Pap. 960905. Warrendale, PA: SAE Int.
- Mackrodt PA. 1980. Zum Luftwiderstand, von Schienenfahrzeugen. *DFVLR AVA IB. 251 80C 08*. Göttingen, Ger.: DFVLR
- Mackrodt PA, Steinheuer J, Stoffers G. 1980. *Aerodynamisch optimale Kopfformen für Triebzüge*, DFVLR IB 152 79 A 27. Göttingen, Ger.: DFVLR
- Maeda T, Kinoshita M, Kajiyama H, Tanemoto K. 1989. Aerodynamic drag of Shinkansen electric car; series 0, series 200, series 100. *Q. Rep. Railr. Tech. Res. Inst.* 30(1):48–56
- Mancini G, Violi AG. 1999. Pressure wave effects of high speed trains running parallel on large and medium sized tunnels of Italian high speed lines. In *Proc. World Congr. Railw. Res., Tokyo*. Tokyo: Railr. Tech. Res. Inst. (CD-Rom)
- Matschke G, Schulte-Werning B, Fauchier C, Gregoire R, Gaylard A. 1999a. Numerical simulation of the flow around a six-coach high speed train. In *Proc. World Congr. Railw. Res., Tokyo*. Tokyo: Railr. Tech. Res. Inst. (CD-Rom)
- Matschke G, Schulte-Werning B, Gregoire R, Beremnger T, Malfatti A, Mancini G. 1999b. TRANSAERO: Results of a European research project in railway aerodynamics. In *Proc. World Congr. Railw. Res., Tokyo*. Tokyo: Railr. Tech. Res. Inst. (CD-Rom)
- Matsuo K, Aoki T, Mashimo S, Nakatsu E. 1997. Entry compression wave generated by a high-speed train entering a tunnel. In *Proc. Int. Symp. Aerodyn. Vent. Veh. Tunn., 9th, Aosta Valley, Italy*. London: ME Publ.
- Miyakawa J, Hosaka S. 1993. Aerodynamic design of frontal shape for JR Maglev train. In *Proc. Int. Conf. Speedup Technol. Railw. Maglev Veh., Yokohama*. pp. 315–19. Tokyo: Jpn. Soc. Mech. Eng.
- Montagne MS. 1973. *Mesure du soufflé provoqué par le passage de la rame TGV 001 a grande vitesse, Inf. Tech. SNCF Equip. Paris No. 12*. Paris: Soc. Natl. Chemins Fr.
- Muhlenberg JD. 1978. *Resistance of a Freight Train to Forward Motion. FRA/ORD I, II, III:78-04*. US Fed. Railr. Admin. Washington, DC
- Pahlke K. 1999a. Application of the standard aeronautical CFD method FLOWer to ETR 500 tunnel entry. In *Proc. Brite/Euram Proj. Symp. Transient Aerodyn. Railw. Syst. Optim., Paris, 1999*, ed. B Schulte-Werning, R Gregoire, A Malfatti, G Matschke. Wiesbaden, Ger.: Verlag Vieweg. In press
- Pahlke K. 1999b. Application of the standard aeronautical CFD method FLOWer to trains passing on open track. In *Proc. Brite/Euram Proj. Symp. Transient Aerodyn. Railw. Syst. Optim., Paris, 1999*, ed. B Schulte-Werning, R Gregoire, A Malfatti, G Matschke. Wiesbaden, Ger.: Verlag Vieweg. In press
- Paradot N, Talcotte C, Willaime A, Guccia L, Bouhadana J-L. 1999. Methodology for computing the flow around a high speed train for drag estimation and validation using wind tunnel experiments. In *Proc. World Congr. Railw. Res., Tokyo*. Tokyo: Railr. Tech. Res. Inst. (CD-Rom)
- Penwarden AD. 1974. *Acceptable Wind Speeds in Towns. BRE CP 1/74*
- Peters JL. 1983. Aerodynamics of high speed trains and Maglev vehicles. In *Impact of Aerodynamics on Vehicle Design*, ed. MA Dorgham, pp. 308–41. London: Inter-science
- Peters JL. 1990a. Bestimmung des aerodynamischen Widerstandes des ICE/V im Tunnel und auf freier Strecke durch Auslaufversuche. *Eisenbahntech.Rundschr.* 39(9):559–64
- Peters JL. 1990b. *Windkanaluntersuchung zum Verhalten von Schienenfahrzeugen Unter Windeinfluss auf Dämmen und Brücken*

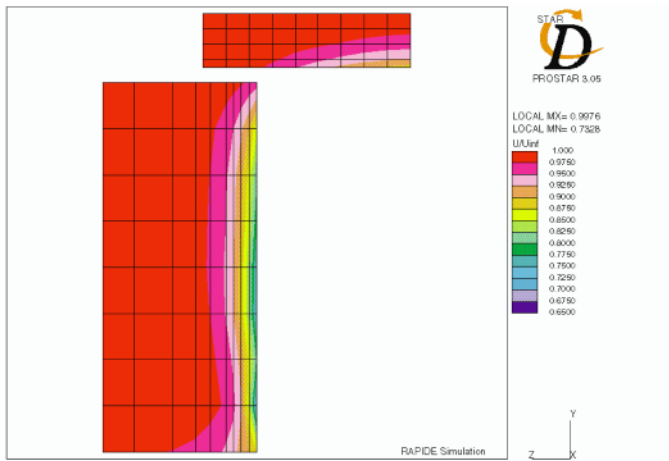
- mit und ohne Schutzeinrichtungen. L333-TB07/90. Ger.: Krauss Maffei Verkehrstechnik
- Pope CW. 1991. The simulation of flows in railway tunnels using 1/25th scale moving model facility. In *Aerodynamics and Ventilation of Vehicle Tunnels*, ed. A. Haerter, pp. 48–56. New York: Elsevier
- Pulliam W, Tyll J, Marchman JF III, Schetz JA. 1996. *Aerodynamics of the AMT Maglev Train Design*. AIAA 96-2476. New York: Am. Inst. Aeronaut. Astronaut.
- Schulte-Werning B, Matschke G, Gregoire R, Johnson T. 1999a. RAPIDE: A project of joint aerodynamics research of the European high-speed rail operators. In *Proc. World Congr. Railw. Res., Tokyo*. Tokyo: Railr. Tech. Res. Inst. (CD-Rom)
- Schulte-Werning B, Matschke G, Williams A, Malfatti A, Mancini G, Pecorni M. 1999b. High speed trains with bogie fairings: European research into reducing aerodynamic drag and noise. In *Proc. World Congr. Railw. Res., Tokyo*. Tokyo: Railr. Tech. Res. Inst. (CD-Rom)
- Schultz M, Sockel H. 1989. Pressure transients in railway tunnels. In *Trends in Applications of Mathematics to Mechanics*, ed. W Schneider, H Troger, F Ziegler, pp. 33–39. Harlow, UK: Longman
- Siclari M, Carpenter G, Ende R. 1993. *The Application of Navier-Stokes Computations to the Design of High-Speed, Low-Drag Magnetically Levitated (Maglev) Vehicle Shapes*. AIAA 93-2950. New York: Am. Inst. Aeronaut. Astronaut.
- Siclari M, Ende R, Carpenter G. 1995. *Navier-Stokes Computations for a Magnetically Levitated Vehicle (Maglev) in Ground Effect*. AIAA 95-1908-CP. New York: Am. Inst. Aeronaut. Astronaut.
- Sockel H. 1996. The aerodynamics of trains. In *Handbook of Fluid Dynamics and Fluid Machinery*, ed. JA Schetz, AE Fuhs, pp. 1721–41. New York: Wiley & Sons
- Stix G. 1992. Air trains. *Sci. Am.* 267(2):102–13
- Suzuki E, Azakami M, Sawano E. 1999. Results of running tests of the MLX01 Yamanshi Maglev test line vehicles. In *Proc. World Congr. Railw. Res., Tokyo*. Tokyo: Railr. Tech. Res. Inst. (CD-Rom)
- Suzuki M. 2000. Computational study on flow-induced vibration of high-speed train in tunnel. *Proc. Int. Conf. Flow Induc. Vib., 7th, Lucerne*
- Suzuki M, Tanemoto K, Maeda T. 1999. Wind tunnel tests on aerodynamic characteristics of vehicles under cross-winds. In *Proc. World Congr. Railw. Res., Tokyo*. Tokyo: Railr. Tech. Res. Inst. (CD-Rom)
- Takaishi T, Zenda Y, Shimizu Y. 1999. Wind tunnel tests for reducing aeroacoustic noise from high-speed trains. In *Proc. World Congr. Railw. Res., Tokyo*. Tokyo: Railr. Tech. Res. Inst. (CD-Rom)
- Takao K, Yoshimura M, Sakai K. 1993. Aerodynamic design of the JR Maglev train frontal shape, part II. In *Proc. Int. Conf. Speedup Technol. Railw. Maglev Veh., Yokohama*, pp. 174–85. Tokyo: Jpn. Soc. Mech. Eng.
- Talotte C, Lazure H, Gradoz Sagawa A. 1999. A cooperation study between RTRI and SNCF on aeroacoustics: numerical simulations and measurements of the aerodynamic noise of car body irregularities. In *Proc. World Congr. Railw. Res., Tokyo*. Tokyo: Railr. Tech. Res. Inst. (CD-Rom)
- Tollmein W. 1927. Luftwiderstand und Druckverlauf bei der Fahrt von Zügen in einem Tunnel. *VDI-Zeit.* 71(6):199–203
- Torii A, Ito J. 1999. Development of the series 700 Shinkansen train-set (improvement of noise level). In *Proc. World Congr. Railw. Res., Tokyo*. Tokyo: Railr. Tech. Res. Inst. (CD-Rom)
- Tsuzuku H, Nakajima S, Sakai K. 1999. Analysis of the relationship between nose shape of high-speed train and the pressure distribution against wayside equipment. In *Proc. World Congr. Railw. Res., Tokyo*. Tokyo: Railr. Tech. Res. Inst. (CD-Rom)
- Tyll J, Liu D-J, Schetz JA, Marchman JF. 1996a. Experimental studies of Maglev aerodynamics. *AIAA J.* 34(2):2465–70

- Tyll JS, Eaglesham MA, Schetz JA, Deisenroth M, Mook DT. 1996b. *An MDO Design Methodology for the Concurrent Aerodynamic/Cost Design of MAGLEV Vehicles*. AIAA 96-4036. New York: Am. Inst. Aeronaut. Astronaut.
- Tyll JS, Schetz JA. 1998. *Concurrent Aerodynamic Shape/Cost Design of Magnetic Levitation Vehicles Using MDO Techniques*. AIAA 98-4935. New York: Am. Inst. Aeronaut. Astronaut.
- Tyll JS, Schetz JA, Mook DT. 1998. *Low-Order methods for Two Dimensional Bluff Bodies in Ground Effect*. AIAA 98-0426. New York: Am. Inst. Aeronaut. Astronaut.
- Vardy AE. 1996a. Aerodynamic drag on trains in tunnels. 1. Synthesis and definitions. *Proc. World Congr. Inst. Mech. Eng.* 210:29–38
- Vardy AE. 1996b. Aerodynamic drag on trains in tunnels. 2. Prediction and validation. *Proc. World Congr. Inst. Mech. Eng.* 210:39–49
- Vardy AE, Anandarajah A. 1982. Initial design considerations for rail tunnel Aerodynamics and thermodynamics. In *Proc. Int. Symp. Aerodyn. Vent. Veh. Tunn., 4th, York, England*, pp. 353–66. Cranfield, UK: BHRA Fluid Eng. Cent.
- Vardy AE, Reinke P. 1999. Estimation of train resistance coefficients in tunnels from measurements during routine operation. *Proc. World Congr. Inst. Mech. Eng.* 213F:71–87
- Werle H. 1969. *Simulation de l'effet de sol au tunnel hydrodynamique. Et film 412*. Paris: ONERA
- Willemsen E. 1997. High Reynolds number wind tunnel experiments on trains. *J. Wind Eng. Ind. Aerodyn.* 69–71:437–47
- Wilt JA, Tyll JS, Schetz JA, Marchman JF III. 1997. *Aerodynamic Performance of Electrodynamic Suspension MagLev Vehicle*. AIAA 97-0821. New York: Am. Inst. Aeronaut. Astronaut.
- Yoshimura M, Saito S, Hosaka S, Tsunoda H. 1999. Characteristics of the aerodynamic brake of the vehicle on the Yamanashi Maglev test line. *Railr. Tech. Res. Inst. Rep.* 13(9):25–28

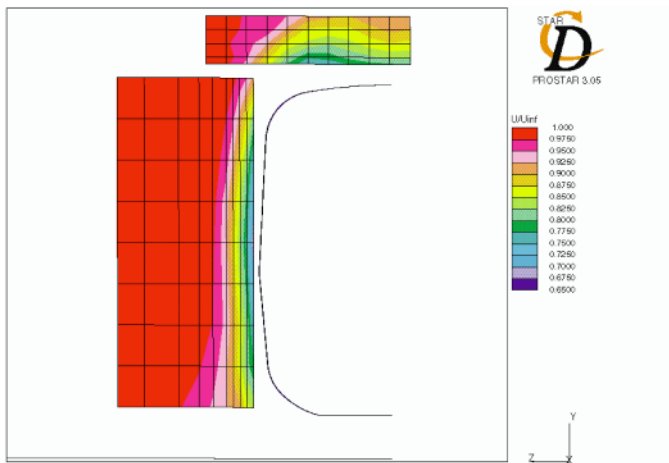


(a)

**Figure 5** Calculations of the flow over an ICE2 train: (a) pressure distribution and streamline patterns over the end car, (b) (next page) predicted longitudinal velocity component distribution at the end of the lead car, and (c) (next page) measured longitudinal velocity component distribution at the end of the lead car. (From Matschke et al 1999a as presented at WCRR '99, with permission of Railroad Technical Research Institute.)



(b)



(c)

Figure 5 (Continued).



**Figure 22** The elevated moving track Maglev test apparatus in the Virginia Tech 6 ft  $\times$  6 ft wind tunnel with an electromagnetic suspension (EMS) system model mounted over the belt.

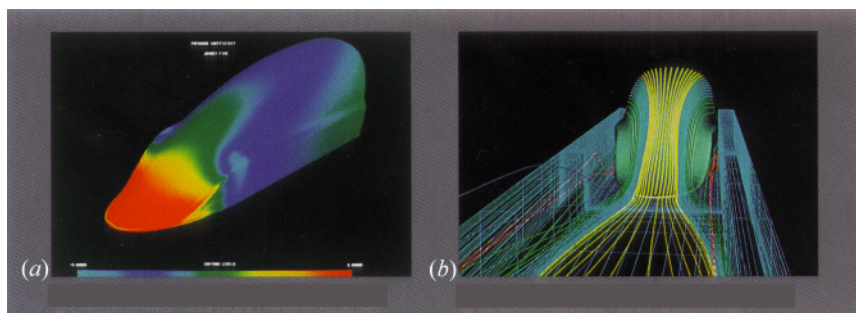


**Figure 28** Predicted flowfield over the duck's bill or double-cusp nose shape for a Maglev vehicle operating in the electrodynamic suspension system rectangular trough. (a) Pressure contours, (b) streamline pattern. (From Miyakawa & Hosaka 1993, with permission of Japanese Society of Mechanical Engineers.)

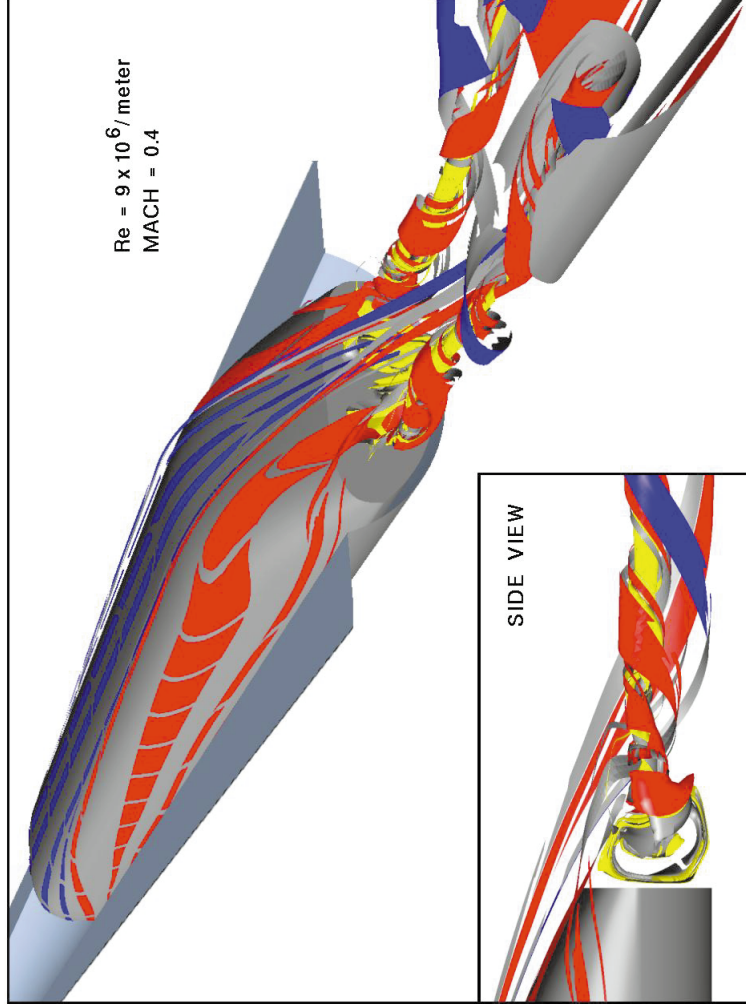


**Figure 30** Reynolds-averaged Navier-Stokes computational fluid dynamic solution for the flow over an electrodynamic suspension system Maglev vehicle design operating in a shallow, U-shaped trough. (From Klopfer & Mehta 1995, with permission of the American Institute of Aeronautics and Astronautics.)



## CONTENTS

---

James Lighthill and His Contributions to Fluid Mechanics, <i>TJ Pedley</i>	1
Steady Streaming, <i>N Riley</i>	43
On the Fluid Mechanics of Fires, <i>Sheldon R Tieszen</i>	67
Experiments on Thermocapillary Instabilities, <i>Michael F Schatz and G Paul Neitzel</i>	93
Robert Legendre and Henri Werlé: Toward the Elucidation of Three-Dimensional Separation, <i>Jean M Détery</i>	129
Surface Pressure Measurements Using Luminescent Coatings, <i>James H Bell, Edward T Schairer, Lawrence A Hand, and Rabindra D Mehta</i>	155
Rosby Wave Hydraulics, <i>ER Johnson and SR Clarke</i>	207
Spin-Up of Homogeneous and Stratified Fluids, <i>PW Duck and MR Foster</i>	231
Extrusion Instabilities and Wall Slip, <i>Morton M Denn</i>	265
Turbulent Relative Dispersion, <i>Brian Sawford</i>	289
Early Work on Fluid Mechanics in the IC Engine, <i>John L Lumley</i>	319
Mechanics of Coastal Forms, <i>Paolo Blondeaux</i>	339
Aerodynamics of High-Speed Trains, <i>Joseph A Schetz</i>	371
Junction Flows, <i>Roger L Simpson</i>	415
Modeling of Fluid-Structure Interaction, <i>Earl H Dowell and Kenneth C Hall</i>	445
Compression System Stability and Active Control, <i>JD Paduano, EM Greitzer, and AH Epstein</i>	491
Spilling Breakers, <i>JH Duncan</i>	519
Shelterbelts and Windbreaks: Mathematical Modeling and Computer Simulations of Turbulent Flows, <i>Hao Wang, Eugene S Takle, and Jinmei Shen</i>	549
Drag Due to Lift: Concepts for Prediction and Reduction, <i>Ilan Kroo</i>	587
Inertial Effects in Suspension and Porous-Media Flows, <i>Donald L Koch and Reghan J Hill</i>	619

## INDEXES

Subject Index	649
Cumulative Index of Contributing Authors, Volumes 1–33	675
Cumulative Index of Chapter Titles, Volumes 1–33	682